This manuscript is a preprint submitted to *Frontiers in Marine Science* and has yet to be formally accepted for publication. Subsequent versions of this manuscript may have slightly different content. If accepted, the final version of this manuscript will be available via the ‘Peer-reviewed Publication DOI’ link.

# Thoughts on prognostically modeling an eddying double-gyre ensemble mean

Andrew Poje, CUNY (poje@math.csi.cuny.edu)
Takaya Uchida, MIPT (uchida.t@mipt.ru)
Quentin Jamet, SHOM (quentin.jamet@shom.fr)
Luolin Sun, FSU (ls24bk@fsu.edu)
Thierry Penduff, CNRS (thierry.penduff@univ-grenoble-alpes.fr)
Bruno Deremble, CNRS (bruno.deremble@univ-grenoble-alpes.fr)
Joseph Schoonover, Fluid Numerics (joe@fluidnumerics.com)
Megan Trapanese, CUNY (meg.trapanese@gmail.com)
Nicolas Wienders, Fluid Numerics (wienders@me.com)
William Dewar†, FSU (wdewar@fsu.edu)

†: deceased

frontiers

# Thoughts on prognostically modeling an eddying double-gyre ensemble mean

**Andrew C. Poje[1,*], Takaya Uchida (内田貴也)[2,3,4], Quentin Jamet[5,6], Luolin Sun (孙洛琳)[2,3,7], Thierry Penduff[3], Bruno Deremble[3], Joseph Schoonover[8], Megan Trapanese[1], Nicolas Wienders[2], and William K. Dewar[3,7]**

[1] *Department of Mathematics, College of Staten Island, The City University of New York, Staten Island, NY, USA*
[2] *Center for Ocean-Atmospheric Prediction Studies, Florida State University, Tallahassee, FL, USA*
[3] *Université Grenoble Alpes, CNRS, IRD, Grenoble-INP, Institut des Géosciences de l'Environnement, Grenoble, France*
[4] *Currently at the Climate Dynamics Laboratory, Center for Earth Sciences, Moscow Institute of Physics and Technology (МФТИ), Dolgoprudny, Russia*
[5] *Service Hydrographique et Océanographique de la Marine (SHOM), Brest, France*
[6] *Institut National de Recherche en Sciences et Technologies du Numérique (INRIA), ODYSSEY group, Plouzané, France*
[7] *Department of Earth, Ocean and Atmospheric Science, Florida State University, Tallahassee, FL, USA*
[8] *Fluid Numerics, Hickory, NC, USA*

Correspondence*:
A. C. Poje; Dept. Mathematics, College of Staten Island, CUNY, 2800 Victory Blvd., Staten Island, NY 10314, USA
andrewpoje@gmail.com

## ABSTRACT

We address the question of separating the ocean's deterministic response to time-dependent forcing from its intrinsic chaotic variability. Because the forcing is neither stationary nor periodic and spatial homogeneity is precluded by both the forcing pattern and boundary conditions, statistical analysis must rely on ensemble averaging. Here, we define this as the arithmetic mean over realizations with equally probable initial conditions. Ideally, one could compute the ensemble mean directly without performing numerous realizations, but this requires knowledge or closure of the second-order statistics — the classical turbulent-closure problem, here recast for a non-equilibrium, geophysical setting. Building on the ideas of nonlinear midlatitude ocean adjustment (Dewar 2003), we examine this problem using idealized quasigeostrophic (QG) double-gyre ensembles subjected to episodic temporal variations in wind forcing. Our objective here is not to develop a subgrid parameterization of unresolved eddies, but rather to construct and test prognostic equations for the ensemble mean itself, using the simplest possible closure assumptions. We find that the performance of ensemble mean closures is highly dependent on the spatiotemporal structure of the forcing. Under slowly varying forcing, approximate closures reproduce the mean evolution reasonably well; under rapidly varying, near-zero-mean forcing, the simplest ensemble-mean closures fail, even at the level of basin-averaged total energy and

enstrophy. In both regimes, the ensemble-mean response is not simply the accumulated imprint of the applied forcing, but instead appears as a continuing, non-equilibrated dialogue between the mean and eddy fields.

**Keywords: Ensemble simulation, ensemble mean, eddy parameterization, quasi-geostrophy, wind-driven gyre, mesoscale eddies**

## 1 INTRODUCTION

Understanding how large-scale ocean circulations adjust to changes in external forcing remains one of the central challenges of geophysical fluid dynamics. At climate scales, the difficulty is not simply that the governing equations are nonlinear and chaotic, but that the ocean's mean state and its intrinsic variability are dynamically entangled. Even under steady forcing, mesoscale turbulence continually feeds back on the large-scale flow, producing a fluctuating equilibrium that is only statistically stationary. When the forcing itself varies in time, this balance is disturbed and the ocean's adjustment reflects both deterministic and stochastic elements of the dynamics. Predicting that adjustment—and, in particular, predicting the evolution of the *ensemble mean* circulation—is the subject of this paper.

In modern climate modeling, such questions are typically recast as problems of parameterization. Global circulation models cannot resolve the full spectrum of mesoscale and submesoscale motions, so their collective influence must be represented through effective diffusivities or flux laws (e.g., Gent and McWilliams, 1990; Gent et al., 1995; Marshall et al., 2012; Mak et al., 2017; Wei et al., 2024). Despite their success in stabilizing coarse-resolution models, these schemes rest on heuristic assumptions—most notably that eddy fluxes act downgradient with respect to mean quantities (Cessi, 2008; Eden and Greatbatch, 2008; Ferrari et al., 2010; Eaves et al., 2025)—whose physical justification remains limited. The ocean's energy pathways are not strictly diffusive, and eddy–mean flow interactions are reciprocal rather than one-way (Vallis, 2006; Arbic et al., 2014; Uchida et al., 2022b, 2024a,b).

An ensemble framework provides a natural language for this problem. Most theoretical descriptions of turbulence, chaos, and climate variability are implicitly ensemble-based (Smagorinsky, 1963; Kraichnan, 1976; Young, 2012; Maddison and Marshall, 2013; Serazin et al., 2015; Leroux et al., 2018; Romanou et al., 2023; Gu et al., 2024). The ensemble average offers a convenient, computationally demanding, approach to separating the externally forced, deterministic system response from its internally generated variability, free from the ambiguities of spatial or temporal filtering (Chen and Flierl, 2015; Penduff et al., 2018; Uchida et al., 2021a). In this sense, the ensemble-mean equations represent the "gold standard" that any eddy parameterization should strive to emulate. At the same time, they define an ideal test bed for examining how well simplified closures capture the feedback between the mean and eddy fields.

Here, rather than attempting to parameterize the unresolved scales directly, we ask a more fundamental question in the case of non-autonomous forcing: *Can one construct a stable dynamical equation for the ensemble mean itself, and evolve it prognostically, using only minimal and physically motivated closure assumptions?* This reframing replaces the subgrid-scale parameterization problem with the broader issue of ensemble-mean predictability. The goal is not to model the small scales, but to test whether the ensemble mean—the "deterministic part" of the turbulent system's response to external forcing—can be predicted without performing a prohibitively large ensemble of realizations.

As a minimal model for the wind-driven gyres of the North Atlantic and Pacific, the quasi-geostrophic (QG) double-gyre model has long served as a paradigm for studying the large-scale response of the ocean to wind forcing (Veronis, 1963). Despite its simplicity, the system captures many of the essential ingredients of the midlatitude ocean circulation: basin-scale recirculations, an energetic eastward jet reminiscent of the Gulf Stream or Kuroshio. In this idealized setting, nonlinear eddy–mean flow interactions can be isolated and examined without the confounding influences of complex topography or buoyancy forcing. The double-gyre model thus provides a compact, easily-computed, and physically interpretable test bed for exploring how large-scale oceanic jets adjust to changes in external forcing.

A substantial body of work has shown that such flows behave as weakly nonlinear oscillators, capable of multiple equilibria, regime transitions, and intrinsic low-frequency variability even under steady forcing (Berloff and McWilliams, 1999; Simonnet, 2005; Berloff et al., 2007). In a broader sense, this behavior exemplifies the idea that the ocean's mean circulation should be viewed as a continuously forced, weakly non-equilibrium system, in perpetual dialogue with its own turbulence—a perspective articulated in earlier studies of midlatitude adjustment and energetics (Dewar, 2003). Here, we revisit that viewpoint using ensembles of QG double-gyre simulations subjected to episodic and oscillatory wind forcing. The QG framework retains the essential baroclinic dynamics and nonlocal eddy feedbacks of the mesoscale ocean (Grooms et al., 2015; Uchida et al., 2021b, 2022a; Deremble et al., 2023), while remaining simple enough to permit fully controlled ensemble experiments over climatically relevant timescales.

Our approach is deliberately simple. We first establish a statistically stationary, eddying double-gyre circulation under steady wind forcing and diagnose its time-mean and fluctuating properties, including the dominant space–time modes obtained via Spectral Proper Orthogonal Decomposition (SPOD; Towne et al. 2018). We then generate large ensembles of simulations subjected to two distinct classes of time-dependent forcing. The first (Case 1) modulates only the amplitude of the large-scale wind stress, producing a basin-scale "pulse" that perturbs the mean jet but leaves its spatial structure unchanged. The second (Case 2) imposes forcing patterns with the same space–time scales as the most energetic eddy modes, effectively driving the system at the fluctuation scales. These two experiments bracket the spectrum of possible eddy–mean interactions, from slowly varying, quasi-equilibrium adjustment to rapidly varying, near-resonant excitation.

To clarify the dynamical controls governing the evolution of the ensemble mean, we derive a simple prognostic closure model and compare its behavior with fully simulated, reference ensembles and with two idealized dynamical-response models. The prognostic *steady-stress* (or *frozen-turbulence*) model replaces the instantaneous Reynolds stresses with their long-time means, providing a minimal closure that predicts the mean field from fixed eddy statistics. The two response models, by contrast, completely neglect the influence of ensemble fluctuations, describing how the mean field adjusts to prescribed forcing in the absence of any eddy contributions. The nonlinear version retains advection of the mean flow but omits coupling to the background state, while the linear version further simplifies the dynamics to a classical $\beta$-plane response. Comparing these simplified models to the fully diagnosed ensemble evolution allows us to assess when, and under what forcing regimes, the ensemble mean can be accurately predicted from limited statistical information.

The results demonstrate that the ability to forecast the ensemble mean depends critically on the temporal and spatial structure of the forcing. When the forcing acts on large, basin-scale structures (Case 1), the ensemble mean responds coherently and the frozen-turbulence closure performs well. When the forcing operates at the scales of the internal eddies (Case 2), energy is rapidly transferred from the mean to the fluctuating field, and all simplified closures fail—even at the level of total energy. In both cases, the ensemble mean is not merely the accumulated imprint of the external forcing, but a dynamically active field engaged in continuous exchange with the underlying turbulence.

These findings highlight the non-equilibrium nature of the oceanic mean state and provide a controlled framework for evaluating closure assumptions in more complex models. While our experiments are idealized, they reveal general principles likely to extend to the real ocean: that ensemble-mean predictability hinges not only on the amplitude of the forcing, but on its time–scale separation from the intrinsic variability of the system. In this sense, the ocean occupies a regime between the two cases examined here—neither fully equilibrated nor purely stochastic—and it is this intermediate regime that presents the greatest challenge for parameterization and prediction.

The remainder of this paper is organized as follows. Section 2 describes the QG model and ensemble methodology, including the SPOD analysis used to identify dominant eddy modes. Section 3 presents the results from the two forcing experiments and evaluates the performance of the three prognostic models. The focus of this paper is on the ensemble mean, referring to past results that emphasize the importance of capturing an accurate mean state in order to accurately capture the eddies (Hallberg, 2013; Mak et al., 2023), but we shall end with some discussion of the eddies in Section 4 and on the broader problem of predicting the large-scale ocean response to time-dependent forcing.

## 2 DATA AND METHOD

Throughout our study, we document the characteristics of an ensemble-mean oceanic jet using the QG wind-driven gyre system. We numerically solve the canonical QG potential vorticity (PV) using the Fast-Fourier Transform (FFT)-based `qgw` solver (Deremble et al., 2024),

$$\frac{\partial q_i}{\partial t} + J(\psi_i, q_i) = \frac{\tau_0}{H_1} F(\boldsymbol{x}, t)\delta_{i,1} + \nu \nabla^2 q_i \,. \tag{1}$$

For two layers, the layer PV, $q_i$, and stream function, $\psi_i$, are non-locally related by:

$$q_1 = \nabla^2 \psi_1 \ + \ \frac{f_0^2}{g' H_1} \left(\psi_2 - \psi_1\right) \ + \ \beta y,$$

$$q_2 = \nabla^2 \psi_2 \ + \ \frac{f_0^2}{g' H_2} \left(\psi_1 - \psi_2\right) \ + \ \beta y.$$

The total energy (per unit density and area) in the domain is given by

$$\mathrm{TE}(t) = \mathrm{KE}(t) + \mathrm{APE}(t) = -\frac{1}{2A} \sum_{i=1}^{2} \int H_i \psi_i q_i \,\mathrm{d}x\,\mathrm{d}y \coloneqq -\{q\psi\} \,, \tag{2}$$

with units $\frac{\mathrm{m}^3}{\mathrm{s}^2}$.

## 2.1 Base Case:

We take the simplest two-layer configuration, $(H_1, H_2) = (400,\, 2600)\,\mathrm{m}$, in a square domain $L_x = L_y = L = 3840\,\mathrm{km}$ on an interior grid $512^2$ ($\Delta x = 7.5\,\mathrm{km}$). The parameters are $f_0 = 9.4 \times 10^{-5}\,\mathrm{s}^{-1}$, $\beta = 1.7 \times 10^{-11}\,\mathrm{m}^{-1}\,\mathrm{s}^{-1}$, and $g' = 0.045\,\mathrm{m\,s}^{-2}$ with a resulting Rossby deformation radius $R_d = 42\,\mathrm{km}$.

The steady, asymmetric wind-stress curl follows Berloff and McWilliams (1999):

$$F(\boldsymbol{x}, t) = F(y) = \frac{\pi}{L}\left\{\sin\left[2\pi\frac{(y - L/2)}{L}\right] - \lambda_0 \cos\left[\pi\frac{(y - L/2)}{L}\right]\right\}\,, \tag{3}$$

with $\tau_0 = 4.0 \times 10^{-5}\,\mathrm{m}^2\,\mathrm{s}^{-2}$ and asymmetry parameter $\lambda_0 = 0.25$. This choice places the zero wind-stress curl at $y \approx 2000\,\mathrm{km}$, slightly breaking the meridional symmetry.

The numerical solution is computed with free-slip boundary conditions for 1,000 years following a 50 year spin-up from rest. The Laplacian diffusivity is $\nu = 75\,\mathrm{m}^2\,\mathrm{s}^{-1}$. The results of steady wind forcing at these parameters show a statistically stationary eddying flow with $\sim$10-15% fluctuations of the total energy about the time-mean state (Fig. 1a). As shown in the spatial plots of the upper layer PV, the flow is strongly eddying. With the time-mean defined by $\overline{g}(\boldsymbol{x}) \overset{\mathrm{def}}{=} \lim_{T\to\infty} \frac{1}{T}\int_0^T g(\boldsymbol{x}, t)\,\mathrm{d}t$, the time-averaged total energy can be decomposed into mean and eddy reservoirs

$$\overline{\mathrm{TE}} = -\left\{\overline{q}\overline{\psi}\right\} - \overline{\{q'\psi'\}} = \mathrm{ME} + \mathrm{EE}$$

and we find a roughly even split, Total energy = 89 units = 53 (mean) + 46 (eddy), between the two components.

To quantify the dominant coherent space–time structures within the statistically stationary eddying regime, we apply Spectral Proper Orthogonal Decomposition (SPOD; Towne et al., 2018) to the potential vorticity and streamfunction fields. SPOD provides an energy-optimal modal basis in the joint spatial–temporal sense: each mode represents a coherent structure oscillating at a single frequency, ranked by its contribution to the total fluctuation energy. In contrast to the traditional spatial POD, which diagonalizes the spatial covariance at zero time lag, or Singular Spectrum Analysis (Ghil et al., 2002) that considers time-lagged covariances, SPOD diagonalizes the cross-spectral density tensor—the Fourier transform of the temporal correlation operator—thereby isolating physically meaningful, frequency-resolved modes. The mathematical details of the implementation, including the energy inner product appropriate to the quasi-geostrophic system, are provided in Appendix A.

For the present analysis, we use the final 1,000 years of statistically steady data. To estimate the cross-spectral statistics with adequate frequency resolution and statistical convergence, the full time series is divided into ten non-overlapping segments of 100 years each. Each block is windowed, Fourier transformed, and used to compute a segment-averaged cross-spectral density matrix from which the SPOD eigenvalues and modes are obtained.

Figure 2 summarizes the results. Panel (a) shows the SPOD eigenvalue spectrum for the leading two modes, $\lambda_1(f)$ (black) and $\lambda_2(f)$ (red), as functions of the frequency. The eigenvalue curves indicate how the total fluctuation energy is distributed over frequency and between coherent spatial patterns. Three frequency bands, highlighted by dashed vertical lines, correspond to distinct dynamical regimes of the flow: a low-frequency, large-scale meandering of the mean jet ($f \approx 0.21$), an intermediate-frequency

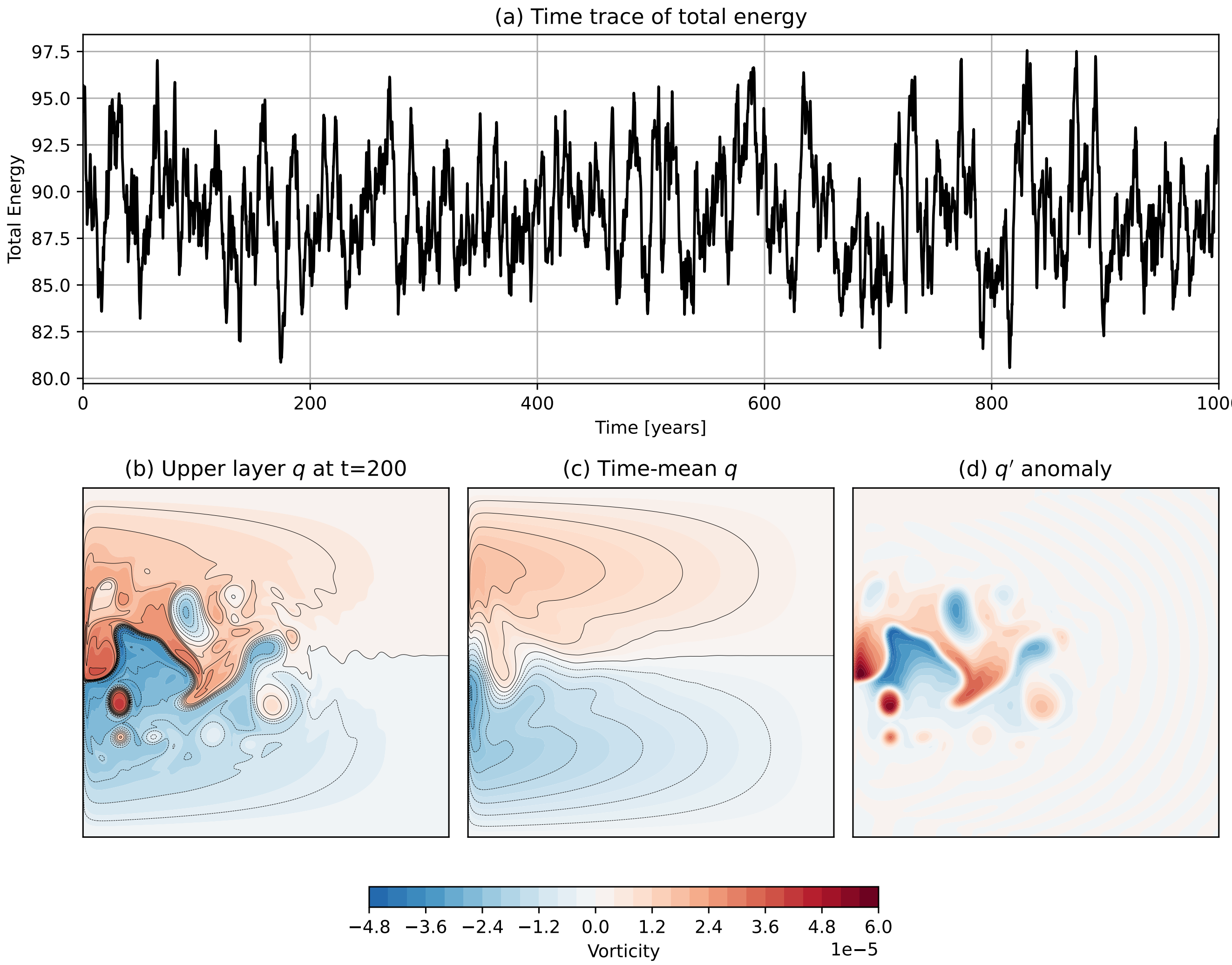


**Figure 1.** (a) 1,000-year time trace of the volume-averaged energy under steady forcing. (b–d) Snapshots of the upper-layer PV at time 200 years (b), the time-mean upper-layer PV, $\overline{q}(\mathbf{x})$ (c), and the fluctuation upper-layer PV, $q'(\mathbf{x}, t)$ at time 50 years (d).

mode associated with gyre-scale recirculation variability ($f \approx 0.65$), and a higher-frequency, mesoscale wave-like pattern ($f \approx 0.95$).

Panels (b–d) show the real parts of the leading SPOD potential vorticity modes, $\Re[\phi_1(\mathbf{x}; f)]$, normalized by their spatial amplitude for the three distinct time-scales. The low-frequency mode is equivalent to the 'gyre-mode' examined in Berloff et al. (2007) encapsulating slow jet migration and changes in the intergyre boundary. The intermediate-frequency mode captures coherent eddy-shedding fluctuations along the western boundary current extensions, while the selected high-frequency mode shows compact, oscillatory vortical features localized in the jet core and recirculation zones. Together, these modes form a natural energetic hierarchy of the flow variability, separating slowly varying gyre–jet adjustment from the more rapid eddy motions that potentially modulate it.

## 2.2 Modeling evolution of the ensemble mean

Statistical stationarity implies, via the ergodic theorem (Birkhoff, 1931; Frisch, 1995; McWilliams, 2006), the equivalence of time and ensemble averages. If the forcing is independent of time, then the time average

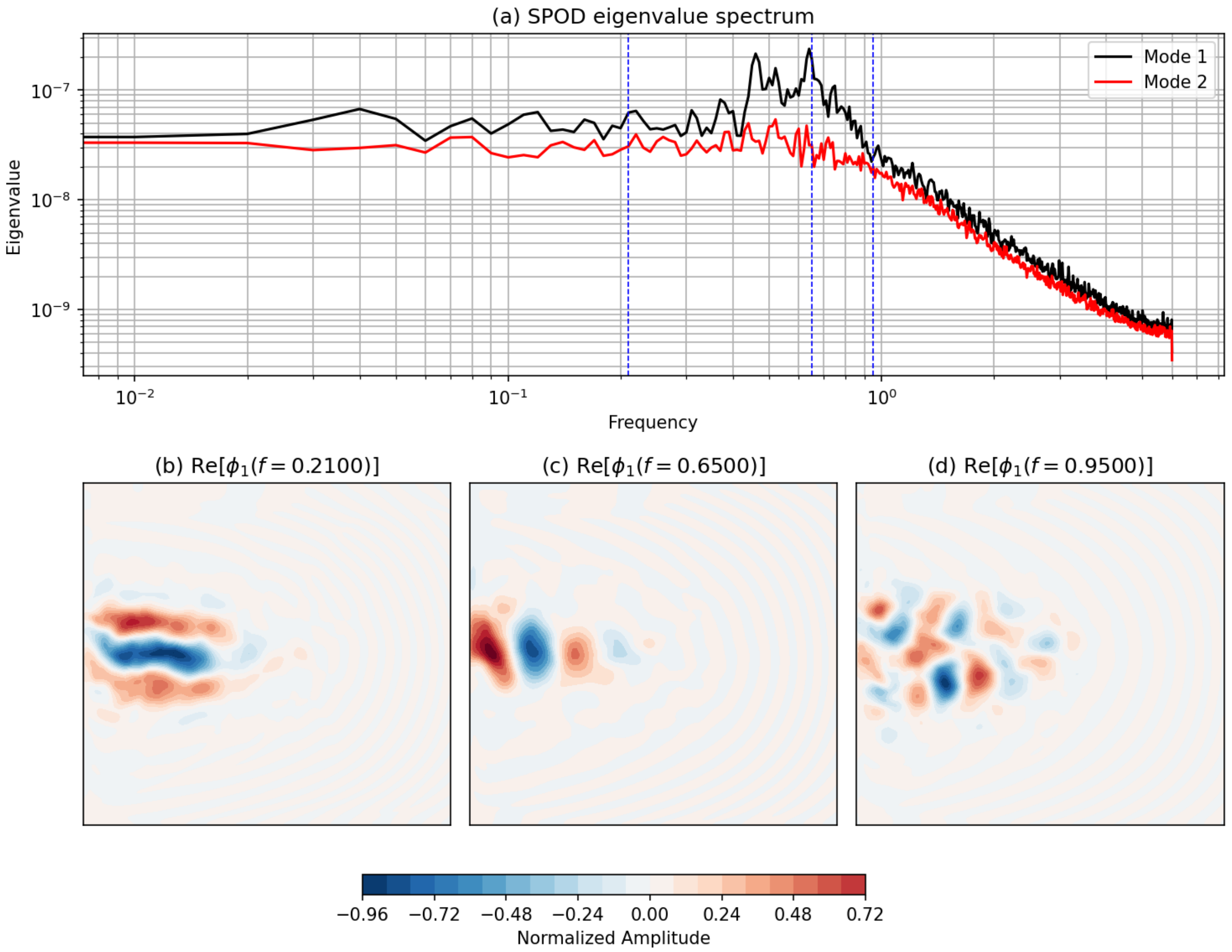


**Figure 2.** Spectral Proper Orthogonal Decomposition from 1,000 years of steady wind forcing. (a) Temporal spectra of first two POD modes (frequencies in units of year$^{-1}$). (b-d) Spatial patterns of the real part of the leading POD pv-mode at three selected frequencies (corresponding to blue lines in (a)).

of Eq. (1) is

$$J(\overline{\psi}_i, \overline{q}_i) = F(y)\delta_{i,1} + \nu\nabla^2\overline{q}_i - \overline{J(\psi_i', q_i')}\,, \tag{4}$$

where $\overline{f}(\boldsymbol{x}) \stackrel{\text{def}}{=} \lim_{T\to\infty} \frac{1}{T}\int_0^T f(\boldsymbol{x},t)\,\mathrm{d}t$ and, for bounded vorticity, the contributions from the time derivative can be made vanishingly small for large enough $T$. Importantly, under steady forcing, the evolution equation for the fluctuations, $\boldsymbol{q}'(\boldsymbol{x},t) = \boldsymbol{q}(\boldsymbol{x},t) - \overline{\boldsymbol{q}}(\boldsymbol{x})$,

$$\frac{\partial q_i'}{\partial t} + \left[J(\overline{\psi}_i + \psi_i', q_i') + J(\psi_i', \overline{q}_i + q_i')\right] = \nu\nabla^2 q_i' + \overline{J(\psi_i', q_i')}\,, \tag{5}$$

contains no direct contribution from the forcing. The fluctuations feel the effect of steady forcing only through its imprint on the time-averaged stream function, potential vorticity, and Reynolds stress terms. This is distinctly different from other situations forced to statistical stationary, perhaps stochastically, by forcing of the form $F_i(\boldsymbol{x},t) = \overline{F}(\boldsymbol{x}) + F_i'(\boldsymbol{x},t)$ where the fluctuations are directly driven. The time-mean decomposition of the flow field shown in the lower panels of Fig. 1 clearly indicates that the details of the instantaneous interior PV at any time is dominated by the intrinsic variability represented by $\boldsymbol{q}'$, but its large-scale structure, of weaker amplitude, is captured by the time mean and mostly reflects the imposed forcing.

Equivalent results hold for temporally periodic forcing with given period, $\mathcal{T}$,

$$F(\boldsymbol{x}, t) = F(\boldsymbol{x}, t + \mathcal{T})\,.$$

In this case, the forcing is invariant under phase averaging,

$$\overline{\overline{g}}(\boldsymbol{x}, \tau) \stackrel{\text{def}}{=} \lim_{M\to\infty} \frac{1}{M} \sum_{j=0}^{M} g(\boldsymbol{x}, \tau + j\mathcal{T})\,,$$

with $\tau \in [0, \mathcal{T})$. Since $\overline{\overline{F}}(\boldsymbol{x}, \tau) = F(\boldsymbol{x}, \tau)$, Eq. (5) holds for the phase-averaged fluctuations which receive no direct input from the periodic forcing.

In the following, we shall develop ensembles of two-layer QG double-gyre simulations which only differ by their initial conditions. Before presenting the results from the numerical experiments, we consider the consequences of aperiodic temporal forcing. Under these conditions, time is no longer a homogeneous direction and the only rigorous averaging operator in the statistical sense is the ensemble average,

$$\langle f(\boldsymbol{x}, t)\rangle \stackrel{\text{def}}{=} \lim_{N\to\infty} \frac{1}{N} \sum_{n=1}^{N} f_n(\boldsymbol{x}, t)\,.$$

Here the individual members of the ensemble, $f_n$, are assumed to be drawn from the set of equally probable flow states at some initial time. By construction, the ensemble mean commutes with any linear spatio-temporal operator and the ensemble mean retains the full dimensionality of any single ensemble member (Chen and Flierl, 2015; Sérazin et al., 2017; Jamet et al., 2022; Uchida et al., 2021b, 2023, 2024a). Mathematical notations are summarized in Table 1.

Although the forcing in Eq. (1) is now time dependent, the fact that it is simply additive implies that $\langle F(\boldsymbol{x}, t)\rangle = F(\boldsymbol{x}, t)$. The evolution of the ensemble-mean PV,

$$\frac{\partial \langle q\rangle_i}{\partial t} + J(\langle\psi\rangle_i, \langle q\rangle_i) = F(y, t)\delta_{i,1} + \nu\nabla^2\langle q\rangle_i - \langle J(\psi_i^\dagger, q_i^\dagger)\rangle\,, \tag{6}$$

differs from that of the time mean only by the retention of the time derivative and, critically, by the statistical definition of the fluctuations comprising the eddy stress term. The corresponding evolution of the ensemble mean energy, $\mathrm{ME} = -\left\{\langle q\rangle\langle\psi\rangle\right\}$ is given by,

$$\frac{d}{dt}\mathrm{ME} = -H_1 \iint \langle\psi_1\rangle F \,\mathrm{d}A \;-\; \mathcal{D} \;+ \Pi \tag{7}$$

where the transfer from mean to eddy reservoirs is

$$T_{M\to E} = -\Pi \;\stackrel{\text{def}}{=}\; -\tfrac{1}{2}\sum_{i=1}^{2} H_i \iint \langle\psi_i\rangle\,\langle J(\psi^\dagger, q^\dagger)\rangle \,\mathrm{d}A. \tag{8}$$

By construction, for identically forced ensemble members, there is no direct contribution of such forcing to fluctuations about the ensemble mean (i.e., the forcing does not appear in the equation corresponding to fluctuations; $\boldsymbol{q}^\dagger \overset{\text{def}}{=} \boldsymbol{q} - \langle \boldsymbol{q} \rangle, F^\dagger = 0$), and the ensemble fluctuations evolve in analogy to Eq. (5).

**Table 1.** Definition of mathematical notations.

| Notation | Description |
|---|---|
| $\overline{(\cdot)}$ | Time mean |
| $(\cdot)' = (\cdot) - \overline{(\cdot)}$ | Temporal fluctuation |
| $\langle \cdot \rangle$ | Ensemble mean |
| $(\cdot)^\dagger = (\cdot) - \langle \cdot \rangle$ | Ensemble fluctuation |
| $\widetilde{(\cdot)} = \langle \cdot \rangle - \overline{(\cdot)}$ | Temporal deviation of ensemble mean from its steady state |
| $\tilde{q}_{\text{FT}}$ | Steady-stress (frozen turbulence) model (11) |
| $\tilde{q}_{\text{LR}}$ | Linear response model (12) |
| $\tilde{q}_{\text{NLR}}$ | Nonlinear response model (13) |

The parameterization problem involves modeling the final expression on the right-hand side of Eq. (6) in terms of known mean quantities: $\langle J(\psi^\dagger, q^\dagger) \rangle = \mathcal{G}(\langle q \rangle)$. Here we consider the ensemble response to episodic changes in the forcing about some steady reference state. The goal is to predict the deviation of the ensemble mean from the given reference steady state whose time-mean statistics are known (based, for example, on our 1,000-year simulation; Fig. 1).

The equation for the deviation of the ensemble mean from the temporal mean, $\tilde{q}_i(\mathbf{x}, t) = \langle q_i \rangle(\mathbf{x}, t) - \overline{q}_i(\mathbf{x})$ (dropping the layer index $i$ for brevity) is

$$\frac{\partial \tilde{q}}{\partial t} + J(\tilde{\psi}, \tilde{q}) + J(\tilde{\psi}, \overline{q}) + J(\overline{\psi}, \tilde{q}) = \mathscr{L}(\tilde{q}) + \widetilde{F} + \left[ \overline{J(\psi', q')} - \underbrace{\langle J(\psi^\dagger, q^\dagger) \rangle}_{=\mathcal{G}(\langle q \rangle)} \right]. \tag{9}$$

$\widetilde{F} = F(y, t) - \overline{F}(y)$ is the temporal deviation of the imposed forcing from its steady value, and $\mathscr{L}(\tilde{q})$ is the linear diffusion term.

Assuming knowledge of the first-order, time-mean statistics ($\overline{q}, \overline{\psi}$), (9) can be closed by adopting a quasi-equilibrium, or frozen-turbulence, approximation (Taylor, 1938; Farrell and Ioannou, 2003; Marston et al., 2016) and simply ignoring any temporal variations in the second-order fluctuation terms. Setting

$$\langle J(\psi^\dagger, q^\dagger) \rangle = \mathcal{G}(\langle q \rangle) \approx \overline{J(\psi', q')}, \tag{10}$$

produces a closed, nonlinear model for $\tilde{q}_{\text{FT}}$ that includes interaction with the underlying time-mean fields,

$$\frac{\partial \tilde{q}_{\text{FT}}}{\partial t} + J(\tilde{\psi}_{\text{FT}}, \tilde{q}_{\text{FT}}) + J(\tilde{\psi}_{\text{FT}}, \overline{q}) + J(\overline{\psi}, \tilde{q}_{\text{FT}}) = \mathscr{L}(\tilde{q}_{\text{FT}}) + \widetilde{F}. \tag{11}$$

Although this closure is by no means "perfect," it should be viewed as a baseline rather than an optimal scheme. In the steady-stress (frozen-turbulence) model, the Reynolds stresses are fixed at their statistically steady values under the control forcing and cannot evolve in response to changes in the ensemble-mean flow. As a result, the model cannot represent the time-dependent transfer of energy or potential vorticity between the ensemble mean and the eddy field. Within that limitation, it nevertheless provides a simple and physically interpretable benchmark, likely competitive with existing prognostic mesoscale parameterizations so long as the modeled regime does not cross a bifurcation point (Simonnet et al., 2003).

Given the common interpretation of the ensemble mean as the forced response of the system (Penduff et al., 2018; Zhao et al., 2021; Narinc et al., 2024; Uchida et al., 2024a; Takasuka et al., 2025), we also consider simple force-response models that completely ignore the effects of the fluctuations; both the fully linear response model, $\tilde{q} = \tilde{q}_{\mathrm{LR}}$,

$$\frac{\partial \tilde{q}_{\mathrm{LR}}}{\partial t} + \beta \frac{\partial \tilde{\psi}_{\mathrm{LR}}}{\partial x} = \mathscr{L}(\tilde{q}_{\mathrm{LR}}) + \widetilde{F}\,. \tag{12}$$

as well as the nonlinear response, $\tilde{q} = \tilde{q}_{\mathrm{NLR}}$,

$$\frac{\partial \tilde{q}_{\mathrm{NLR}}}{\partial t} + J(\tilde{\psi}_{\mathrm{NLR}}, \tilde{q}_{\mathrm{NLR}}) = \mathscr{L}(\tilde{q}_{\mathrm{NLR}}) + \widetilde{F}\,. \tag{13}$$

Comparison of the full ensemble-mean response, $\langle q \rangle$, to $\tilde{q}_{\mathrm{FT}}$, $\tilde{q}_{\mathrm{NLR}}$ and $\tilde{q}_{\mathrm{LR}}$ quantifies the relative importance of nonlinearity, time-mean interactions and temporal variations in the Reynolds stresses in response to changes in the forcing.

## 3 RESULTS

In what follows, we investigate how the statistically stationary eddying flow responds to episodic changes in the imposed forcing. As shown above, for identically forced ensemble members, deviations from the steady forcing act only on the ensemble mean. The spatial–temporal structure of the mean field determines the pathways through which energy and potential vorticity anomalies are communicated to, and subsequently redistributed by, the eddy field. Here we consider two extreme cases.

In Case 1, the spatial form of the wind stress is fixed, but the amplitude varies in time as

$$\tau_0 \to \tau_0 \left(1 + b(t; a, t_0, \sigma)\right) \,,$$

where $b(t)$ is the Gaussian

$$b(t; a, t_0, \sigma) = a \exp\left(\frac{(t - t_0)^2}{2\sigma^2}\right).$$

In Case 2, by contrast, the spatial and temporal scales of $\tilde{F}(\mathbf{x}, t)$ are chosen to roughly match those of the most energetic eddy structures identified through the SPOD analysis of the statistically steady flow. This formulation allows us to explore how the ensemble-mean circulation responds when externally driven by patterns that resemble the internal, energetic modes of the turbulent flow, rather than by a basin-scale modulation of the steady wind stress.

This forcing framework—examined here in the ensemble-mean context—is closely related to that introduced by Dewar in his study of nonlinear midlatitude ocean adjustment (Dewar, 2003). Our Case 1 is essentially a “turn-on/turn-off” experiment, while Case 2 corresponds conceptually to his periodically forced regime, in which the spatial and temporal structure of the forcing is tuned to resonate with the intrinsic variability of the system.

### 3.1 Case 1: Change in wind-stress amplitude

We begin with the simpler case of a time-dependent modulation of the large-scale wind stress amplitude. An ensemble of initial conditions is constructed by randomly sampling the 1,000-year time series in Fig. 1 120 times with a minimum of five years between each sample. Namely, we create a 120-member ensemble differing only by their initial conditions. The parameters of the Gaussian bump are $a = 4.0$, $t_0 = 3$, and $\sigma = 1/2$ years. Each realization is integrated for 20 years under this forcing history, which represents a temporal "blip"—a short-duration, basin-wide amplification of the same spatial forcing pattern that maintains the steady double-gyre circulation.

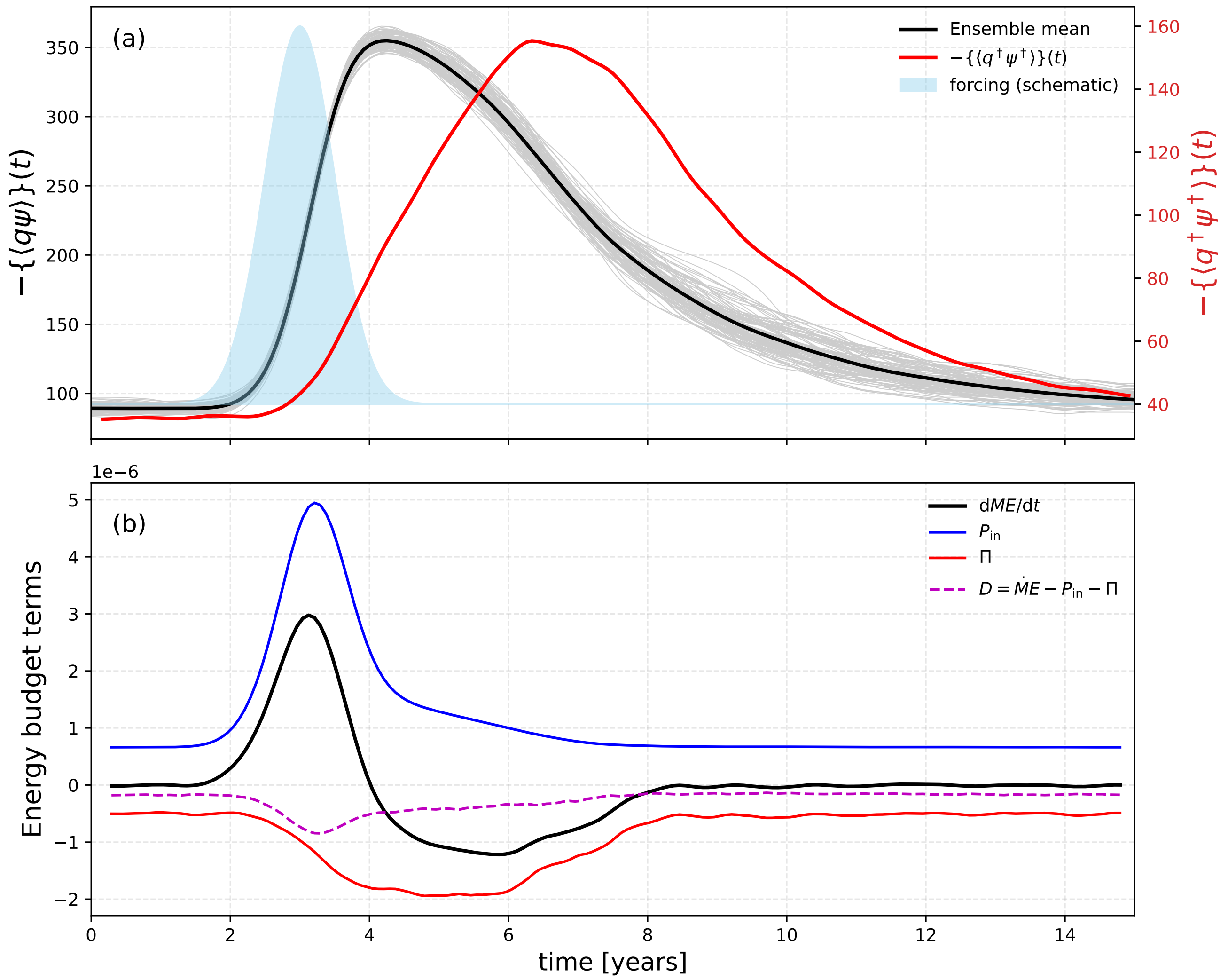


**Figure 3.** Case 1: (a) Left $y$ axis shows evolution of the total energy for 120 individual ensemble members (light grey curves) and the ensemble mean of total energy (black). Right $y$ axis shows evolution of the ensemble mean eddy energy (red). Temporal dependence of $\tilde{F}(t)$ shown schematically in blue. (b) Evolution of the components of reference ensemble mean energy budget.

Figure 3 summarizes the ensemble-mean energetics. Panel (a) shows the evolution of the total energy for all ensemble members (light grey) together with the ensemble-mean total energy (black) and the ensemble-mean eddy energy (red). The blue curve indicates the temporal shape of the imposed forcing anomaly $\tilde{F}(t)$.

As shown in Fig. 3a, the fourfold increase in wind stress produces a rapid, roughly 350% rise in total energy, peaking about one year after the maximum forcing. This response is followed by a slower relaxation back toward the equilibrium value. Decomposition of the energy into mean and eddy components (Fig. 3a) indicates that the injected energy is directly fed into the ensemble-mean component, with little short-term change in the eddy reservoir during the brief forcing pulse.

Panel (b) shows the diagnosed terms of the ensemble–mean energy budget,

$$\frac{d}{dt}\mathrm{ME}(t) = P_{\mathrm{in}}(t) + \Pi(t) + D(t),$$

where $\mathrm{ME}(t) \overset{\mathrm{def}}{=} -\{\langle q \rangle \, \langle \psi \rangle\}$ is the basin–mean energy, $P_{\mathrm{in}}(t)$ is the wind–work input, $\Pi(t)$ is the reversible exchange between the mean and eddy reservoirs (negative values denote mean$\to$eddy transfer), and $D(t) \leq 0$ is the mean–field dissipation, diagnosed as the residual $D = d\mathrm{ME}/dt - P_{\mathrm{in}} - \Pi$. During the pulse $P_{\mathrm{in}}$ rises sharply and accounts for nearly all of the positive $d\mathrm{ME}/dt$, while $\Pi$ remains small: the wind energizes the mean circulation directly. After the pulse, $P_{\mathrm{in}}$ relaxes toward its control value but $\Pi$ becomes strongly negative, indicating a delayed mean$\to$eddy cascade; $d\mathrm{ME}/dt$ crosses zero when $|\Pi| + |D|$ exceeds $P_{\mathrm{in}}$, and the mean energy decays on the basin–adjustment timescale. This two–stage sequence—direct wind input to the mean followed by a lagged transfer to the eddies—explains the phase offset between the input forcing and the peaks in $\mathrm{TE}(t)$ and eddy energy seen in Fig. 3(a). The magnitude of the direct mean dissipation is small and in phase with the mean response.

To assess model performance, we track the basin-integrated energy of the ensemble mean, $\mathrm{ME}(t) \overset{\mathrm{def}}{=} -\{\langle q \rangle \langle \psi \rangle\}$, and two field-level skill metrics between modeled and reference upper-layer ensemble-mean PV: an area-weighted RMS error and a spatial pattern correlation $r(t)$,

$$\mathrm{RMS}(t) = \left[ \frac{1}{A} \iint \left( \langle q \rangle_{\mathrm{mod}} - \langle q \rangle_{\mathrm{ref}} \right)^2 \mathrm{d}A \right]^{1/2},$$

$$r(t) = \frac{\iint \left( \langle q \rangle_{\mathrm{mod}} - \overline{\langle q \rangle_{\mathrm{mod}}} \right) \left( \langle q \rangle_{\mathrm{ref}} - \overline{\langle q \rangle_{\mathrm{ref}}} \right) \mathrm{d}A}{\sqrt{\iint \left( \langle q \rangle_{\mathrm{mod}} - \overline{\langle q \rangle_{\mathrm{mod}}} \right)^2 \mathrm{d}A} \, \sqrt{\iint \left( \langle q \rangle_{\mathrm{ref}} - \overline{\langle q \rangle_{\mathrm{ref}}} \right)^2 \mathrm{d}A}}, \tag{280}$$

where $\langle q \rangle_{\mathrm{mod}} \overset{\mathrm{def}}{=} \tilde{q}_{\mathrm{mod}} + \overline{q}$ represents the modeled ensemble mean from (11)–(13) and $\langle q \rangle_{\mathrm{ref}}$ is the reference ensemble mean diagnosed from the actual ensemble computations. Comparisons of the three models are shown in Fig. 4.

All three models reproduce the rapid, one-year-lagged rise of $\mathrm{ME}(t)$ and its slower decay (Fig. 4a), as expected for basin-scale forcing that projects directly onto the steady mean state. Larger differences are seen in the field-level metrics (Fig. 4b,c): FT has the smallest RMS and the highest $r(t)$ throughout most of the 20-year window; LR shows intermediate skill—tracking the early adjustment but losing correlation during the recovery as phase and amplitude drift; NLR performs worst, overshooting the peak response and diverging thereafter. The largest decline in $r(t)$ for steady-stress model occurs during the period of strong mean-eddy coupling shown in Fig. 3b.

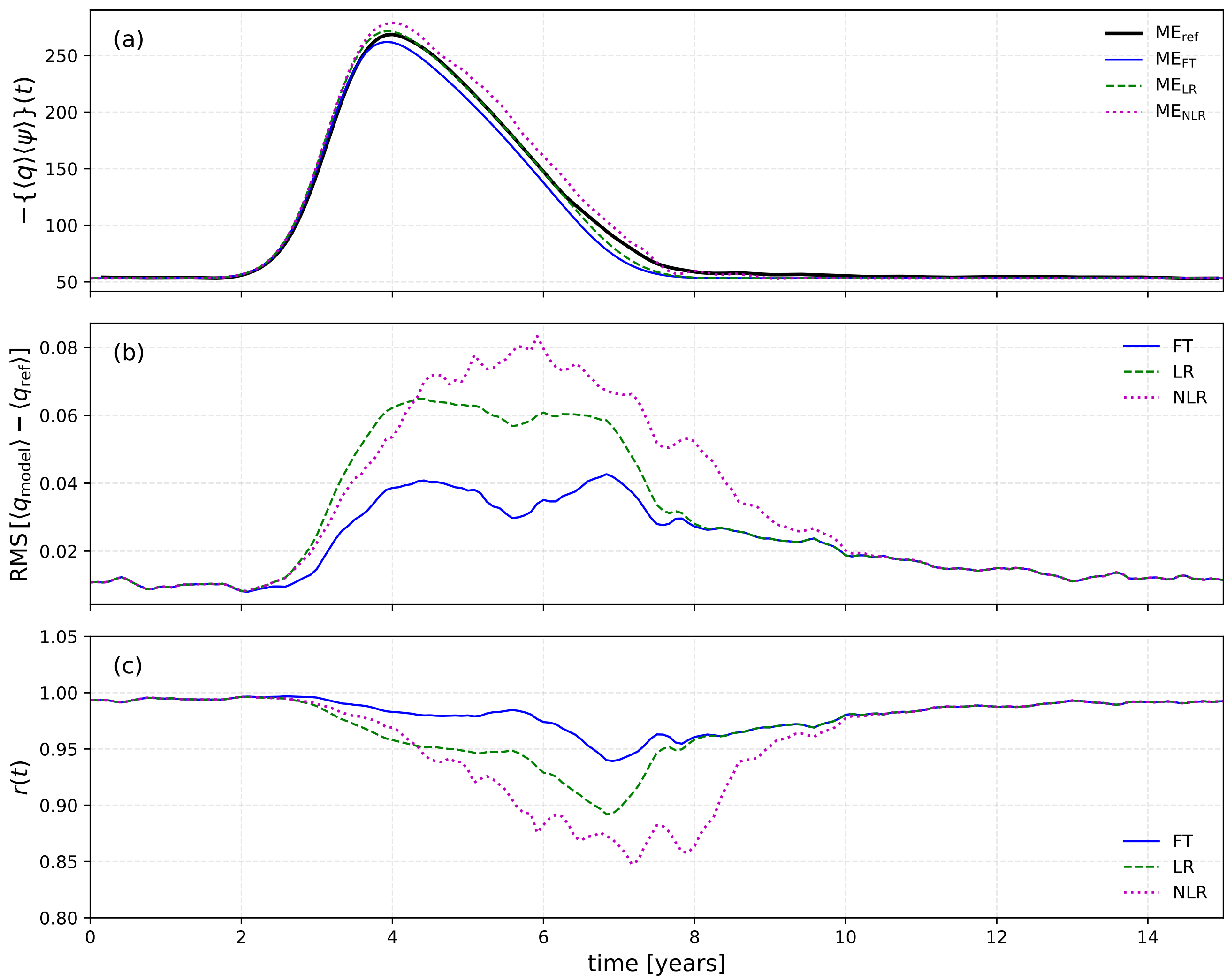


**Figure 4.** Case 1: Comparison between the directly computed and modeled upper-layer potential vorticity response to time-dependent forcing. **(a)** Mean energy $-\{\langle q\rangle\langle\psi\rangle\}(t)$ from the reference ensemble (black) and from the frozen-turbulence (FT, blue), nonlinear-response (NLR, magenta), and linear-response (LR, green) models. **(b)** Root-mean-square difference $\mathrm{RMS}[\langle q\rangle_{\mathrm{model}} - \langle q\rangle_{\mathrm{obs}}]$ between the modeled and reference upper-layer ensemble mean fields. **(c)** Spatial pattern correlation $r(t)$ between modeled and reference ensemble mean fields.

Snapshots of the upper-layer ensemble-mean PV fields (Fig. 5) explain the skill ranking. The diagnosed ensemble mean ($\langle q\rangle_{\mathrm{ref}}$, first column) exhibits a coherent intensification and northward shift of the jet during the forcing pulse, followed by a gradual relaxation toward its pre-forcing state. The steady-stress model ($\langle q_{\mathrm{FT}}\rangle$, second column) captures this large-scale adjustment, though with a somewhat broader and more diffuse jet core—a direct consequence of neglecting time-dependent eddy feedbacks. Because it retains the time-mean Reynolds stresses, it still "knows" the structure and stabilizing influence of the mean flow, producing the correct, bounded evolution.

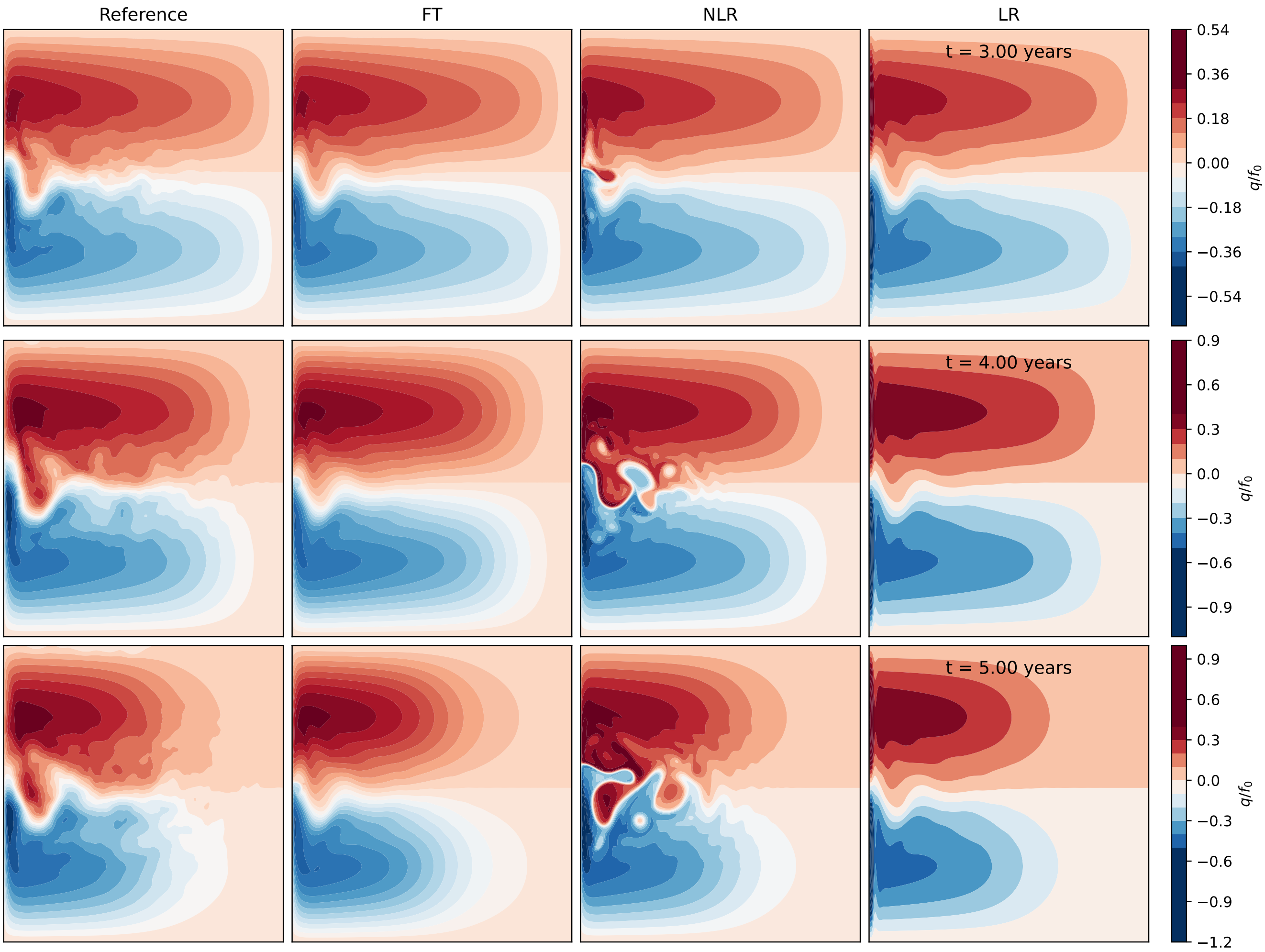


**Figure 5.** Case 1: Instantaneous snap-shots of the reference and modeled upper layer ensemble-mean PV, $\langle q\rangle_{\mathrm{ref}}/f_0$ and $\langle q\rangle_{\mathrm{mod}}/f[= (\tilde{q}_{\mathrm{mod}} + \overline{q})/f_0]$ respectively, at three time steps (at years three, four and five; cf. Fig. 3). The first second column from the left corresponds to the 'true' ensemble mean, second column to $\langle q_{\mathrm{FT}}\rangle$, third column to $\langle q_{\mathrm{NLR}}\rangle$ and the right column to $\langle q_{\mathrm{LR}}\rangle$. Colormaps and contour levels are identical across each row.

The nonlinear response model ($\langle q_{\mathrm{NLR}}\rangle$, third column) behaves very differently. Lacking any reference to the background mean state or its stabilizing Reynolds-stress divergence, it reacts to the large forcing amplitude by developing its own mesoscale instabilities. Within a few years the field becomes fully eddying, effectively spinning up a new chaotic turbulent circulation unrelated to the directly computed ensemble-mean adjustment. In this sense, its apparent realism—nonlinear eddy activity—is misplaced, as it arises from the absence of mean-flow anchoring rather than from correct eddy–mean dynamics.

The linear response model ($\langle q_{\mathrm{LR}}\rangle$, fourth column) remains stable but produces overly smooth and symmetric PV anomalies. Because the evolution retains the $\beta$-term, even weak zonal variations excited by the boundaries generate barotropic Rossby waves. The Gaussian temporal pulse excites a westward-propagating packet with (barotropic) phase speed $c_R = \frac{\beta}{k^2+l^2}$. Without mean-flow absorption or nonlinear redistribution, this wave activity reflects at the western boundary where $c_R \to 0$, leading to the excessive PV buildup along the western wall visible in the linear model. In contrast, in the fully eddying ensemble and the steady-stress model, westward energy fluxes are absorbed by eddy stresses and re-emitted more isotropically, preventing this unrealistic accumulation.

Although all three models produce comparable basin-integrated energy curves, only those that maintain an explicit coupling to the time-mean flow reproduce the observed, coherent, and reversible ensemble-mean response. The linear model, dominated by $\beta$-plane Rossby adjustment and diffusion, remains overly smooth and accumulates PV at the western boundary, while the unconstrained nonlinear model destabilizes and spawns its own eddy field. The steady-stress closure, though neglecting temporal feedbacks, best captures the large-scale, bounded evolution of the ensemble mean.

The response in Case 1 thus reflects how the ensemble mean adjusts when the external perturbation acts at the same spatial scales as the time-mean forcing. In the next experiment, we shift perspective: the forcing itself is designed to operate on eddy scales, with spatial and temporal organization patterned after the dominant SPOD mode of the turbulent flow. This coherent eddy-scale (SPOD-mode) forcing provides a complementary test of how the ensemble mean responds when driven not by basin-wide modulation but by forcing at scales that characterize its intrinsic eddy variability.

## 3.2 Case 2: Coherent eddy-scale (SPOD-mode) forcing

We next consider a perturbation whose spatial and temporal structure is patterned after the most energetic eddy variability of the statistically steady flow. As before, an ensemble of 120 identically forced integrations is performed, differing only by their initial conditions drawn from the long steady-state record. In this case, $\tilde{F}(\boldsymbol{x}, t)$ is chosen to act on time-space scales consistent with the leading SPOD mode at $f = 0.65$ year$^{-1}$.

As shown in Fig. 6a,c, the leading SPOD mode represents an oscillatory jet-centered structure. The mode exhibits a Gaussian-like envelope in the meridional direction, centered on the inter-gyre jet, and a quasi-sinusoidal variation in the zonal direction with an effective wavelength of about one quarter of the basin width. Roughly two complete zonal oscillations are visible within the first half of the domain, with the amplitude decaying downstream along the jet. To obtain a compact and analytically tractable representation, we idealize this pattern as a simple dipole in $x$ modulated by a Gaussian in $y$ giving the fields $A(x, y)$ and $B(x, y)$ shown in panels (b) and (d). This abstraction retains the dominant spatial phase relationship and scale of the coherent mode.

These two fields are then combined to define the time-dependent forcing,

$$\tilde{F}(\boldsymbol{x}, t) = \tau_1 \, h(t - t_0) \left\{ A(x, y) \cos\big(2\pi\omega(t - t_0)\big) + B(x, y) \sin\big(2\pi\omega(t - t_0)\big) \right\} .$$

As shown in the insets on panels (b,d), the forcing oscillates with period 1.5 years, and $h(t)$ is a smooth bump-function envelope active for $t \in [1, 9]$ years, giving 6 cycles of the forcing. The amplitude, $\tau_1$ is set to $10\tau_0$.

Figure 7a shows the basin-averaged energetics for the full ensemble. Because all ensemble members experience identical forcing, external work enters only through the ensemble-mean equations. Nevertheless, this energy is almost immediately transferred to the eddy component through nonlinear eddy–mean interactions. The modest growth in total energy over the forcing period is due to the increase in the eddy component, not the mean. Panel (b) decomposes the anomaly energy budget into its principal components—rate of change, wind-work, and mean–eddy transfer—revealing that the externally supplied power is almost immediately exported to the eddy field. In contrast to Case 1—where injected energy first

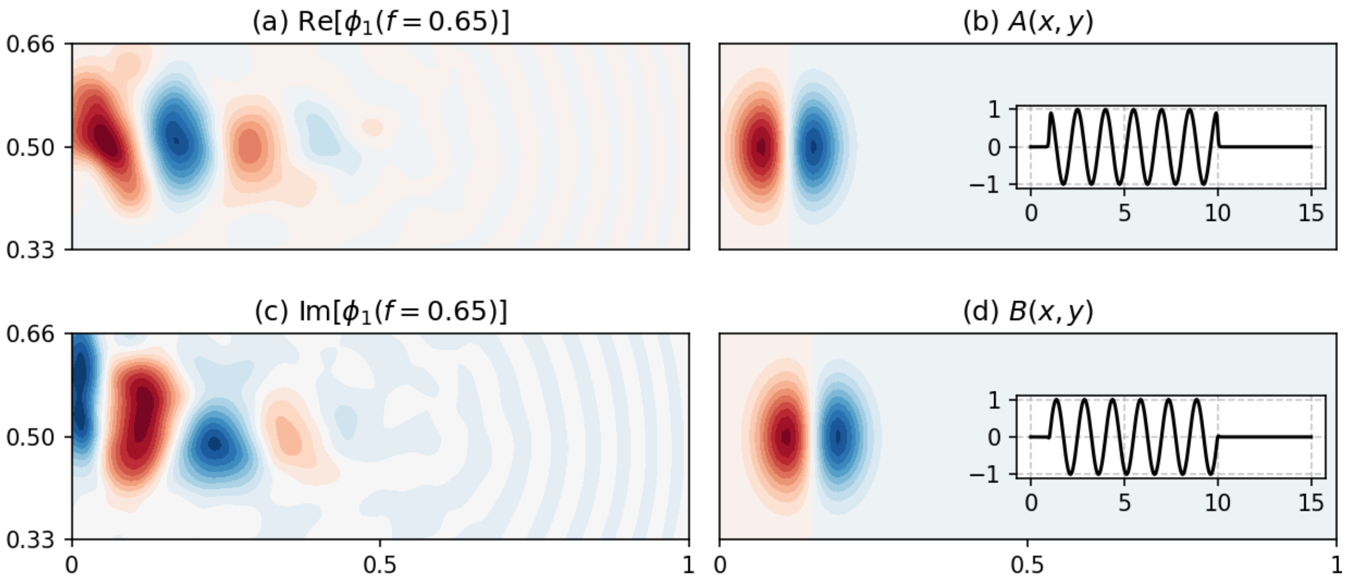


**Figure 6.** Forcing function for Case 2. (a,c) Real and Imaginary parts of the most energetic spatial SPOD modes (only $y \in [1/3, 2/3]L_y$ shown). (b,d) Idealized $A(x,y)$, $B(x,y)$ with temporal dependence inset.

accumulated in the mean reservoir and only later cascaded into the fluctuating reservoir, the response here exhibits a persistent and efficient mean$\rightarrow$eddy energy transfer operating continuously during the forcing window. As a result, the anomaly mean response is not merely a phase-lagged copy of the forcing but instead cycles at a higher, internally determined, frequency.

As shown in Fig. 8, the simple prognostic models for $\tilde{q}$ are incapable of capturing such dynamics. Each absorbs the applied power directly into the mean equation but lacks any mechanism to transfer that energy to the evolving eddy field. Consequently, all three clearly overpredict the ensemble-mean energetics:

1. The **linear response model** integrates the oscillatory forcing into a large, smooth rise of mean energy, tracking the envelope $h(t)$. Without nonlinear redistribution, the $\beta$-term merely drives westward-propagating barotropic and baroclinic Rossby packets that reflect at the western wall, amplifying the mean field still further.
2. The **nonlinear response model**, though containing self-advection, still lacks coupling to the underlying steady eddy stresses. It therefore traps the injected energy within the mean until perturbations reach finite amplitude, at which point new mesoscale instabilities emerge and the model spins up a spurious, self-sustained eddy field.
3. The **steady-stress prognostic model** performs best. Because it includes the spatial structure of the statistically steady Reynolds-stress divergence, it can redistribute the injected anomalies along mean-flow pathways, exporting energy toward regions of enhanced dissipation.

While RMS comparisons of $\tilde{q}_{\text{ref}} (= \langle q \rangle_{\text{ref}} - \overline{q})$ and $\tilde{q}_{\text{mod}}$ (Fig. 8b) are roughly consistent with those for the energy, all three models yield very similar $r(t)$ curves that oscillate between positive and negative values ($\approx \pm 0.5$). As seen in Fig. 7b, the directly computed ensemble responds to the periodic forcing at its own internal frequency. By contrast, the models lack a time-dependent mean$\leftrightarrow$eddy pathway, and their responses are inherently locked to the forcing frequency, producing alternating spatial alignment of the model and reference ensemble-mean fields (Fig. 9).

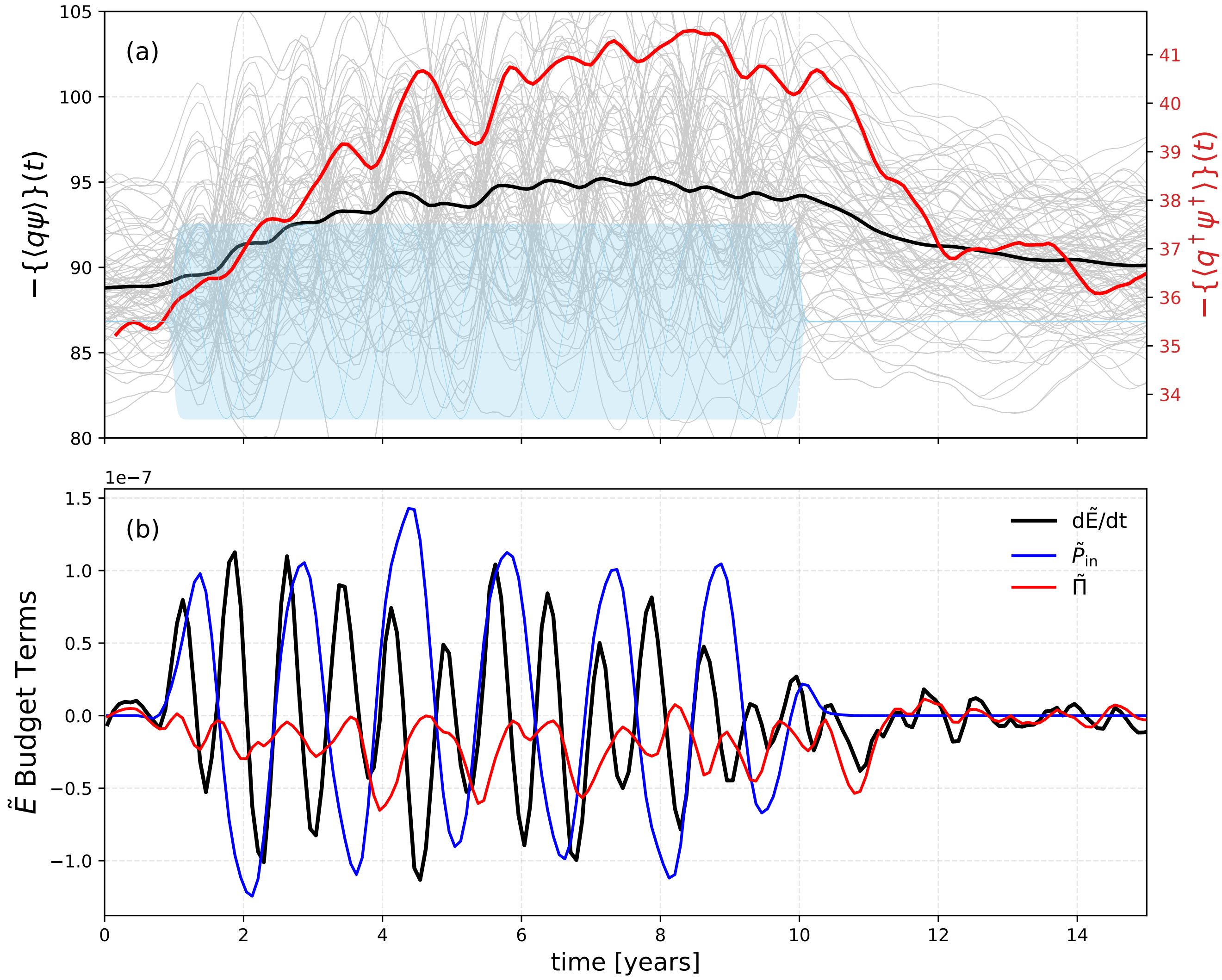


**Figure 7.** Case 2: Energetic response to the time-dependent wind-stress forcing. **(a)** Reference ensemble-mean total energy, $-\{\langle q\psi\rangle\}(t)$ (black) and eddy energy $-\{\langle q'\psi'\rangle\}(t)$ (red), computed from 120 ensemble members (thin grey lines). The shaded region denotes the temporal envelope of the oscillatory wind forcing. **(b)** Corresponding anomaly energy budget terms showing the rate of change $\mathrm{d}\tilde{E}/\mathrm{d}t$ (black), the wind-work input $\tilde{P}_{\mathrm{in}}$ (blue), and the mean-to-eddy energy transfer $\tilde{\Pi}$ (red). Both panels share the same time axis; the forcing period in (a) is vertically aligned with the response in (b).

Case 2 highlights the qualitative change in the energy pathways when the external forcing acts at eddy scales. Even though the external work formally enters only in the ensemble-mean equation, in the reference ensemble solution that energy is rapidly and continuously transferred to the eddy field through nonlinear eddy–mean coupling. Forced perturbations of the ensemble mean remain weakly energetic, serving primarily as an intermediary through which energy is injected and immediately exported to the eddies. All three prognostic models fail to capture this redistribution: Forced to absorb the injected energy directly, they overpredict the amplitude of the mean response by large factors. The steady-stress model, by retaining the stationary eddy-stress divergence, is able to advect the perturbations away and limit their accumulation, but it still lacks the explicit feedback necessary to reproduce the observed eddy energy growth.

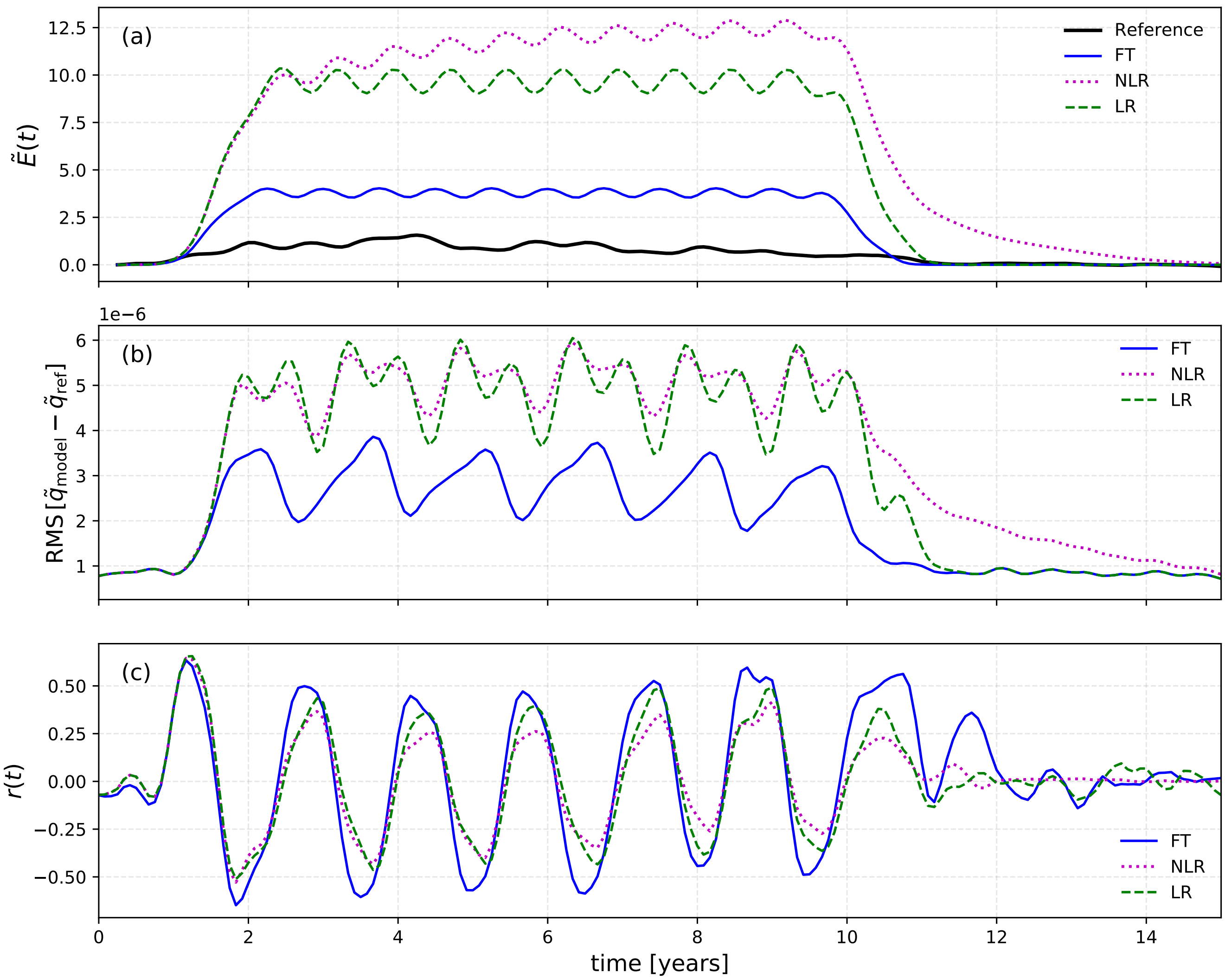


**Figure 8.** Case 2: **(a)** Mean anomaly energy $-\{\tilde{q}\tilde{\psi}\}(t)$ from the reference ensemble (black) and from the frozen-turbulence (FT, blue), nonlinear-response (NLR, magenta), and linear-response (LR, green) models. **(b)** Root-mean-square difference $\mathrm{RMS}[\tilde{q}_{\mathrm{model}} - \tilde{q}_{\mathrm{ref}}]$ between the modeled and reference upper-layer anomaly fields. **(c)** Spatial pattern correlation $r(t)$ between modeled and reference upper layer anomalies.

These results emphasize that the dominant pathway of adjustment at eddy scales is the continual mean→eddy transfer, not storage within the mean circulation. Accurately capturing this behavior requires explicit representation of time-dependent eddy feedbacks, which are absent in all simplified closures tested here.

## 4 CONCLUSIONS AND DISCUSSION

In studying parameterizations of oceanic turbulence, one must decide what is meant by the “mean” and by the “eddies” whose effects are to be represented. A common practice in coarse–grained modeling is to define these quantities through a spatial or temporal filtering operator, leading to filtered–residual equations that depend explicitly on the filter scale. This procedure inevitably introduces inconsistencies in how forcing terms appear in the mean and residual equations. Applying the spatial filter with length scale $\ell$ to the forcing $F$ would result in its filtered $\overline{F}^{\ell}$ and residual $F - \overline{F}^{\ell}$ terms appearing in the equations. This would

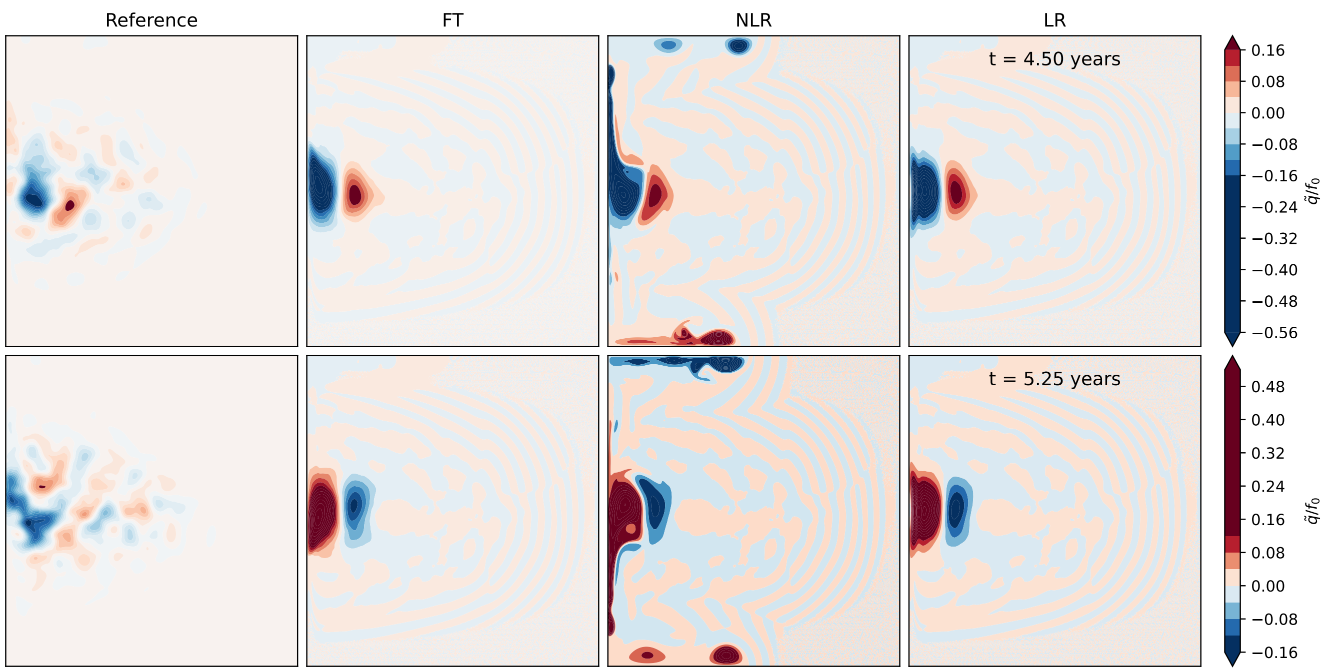


**Figure 9.** Case 2: Reference and modeled upper layer PV anomaly, $\tilde{q}_{\text{ref}} = \langle q \rangle_{\text{ref}} - \overline{q}$ and $\tilde{q}_{FT}, \tilde{q}_{LR}, \tilde{q}_{NLR}$ respectively, at opposite phases of forcing cycle ($4.5$ and $5.25$ years). Colormaps and contour levels are identical across each row.

imply that $F - \overline{F}^{\ell}$ injects variability to the residual flow. By contrast, the ensemble formulation used here provides a mathematically consistent decomposition: The external forcing enters only the ensemble–mean equation, $\langle F \rangle = F$, while the fluctuations evolve without direct forcing. In this sense, the ensemble mean represents the deterministic, externally forced response of the system, and the fluctuations represent its intrinsic, chaotic variability. Such a statement is reminiscent of the Green's function approach (Lembo et al., 2020; Haine et al., 2025), which would in theory allow one to predict the immediate response by the system to any forcing. The deterministic and chaotic variability, however, are dynamically coupled, and their exchange of energy and potential vorticity renders the overall statistics intrinsically unequilibrated (Pierini, 2020; Fedele et al., 2021).

We have tested this paradigm in perhaps the simplest possible nonlinear "ocean" model—a two-layer QG double-gyre circulation—by constructing ensembles of identically forced simulations subject to episodic changes in the wind stress. Two experiments were designed to highlight opposite ends of the spectrum of mean–eddy interaction. In **Case 1**, a basin-scale modulation of the wind stress amplitude produces a clear and intuitive response: The ensemble mean adjusts directly to the imposed change in forcing, and energy subsequently flows from the mean reservoir into the fluctuations as the system relaxes. In **Case 2**, the forcing varies at the observed eddy scales, patterned after the dominant SPOD mode of the turbulent state. Here, the ensemble mean response is highly muted—the injected power is almost immediately transferred to the fluctuating fields, and the mean acts mainly as an intermediary in a continuous mean$\rightarrow$eddy energy exchange. These contrasting cases emphasize that even in a nominally forced–dissipative equilibrium, the ensemble statistics remain far from equilibrium when the forcing varies in time or scale.

To interpret these results, we compared three simple prognostic models for the ensemble mean:

(i) A "steady-stress" model in which the instantaneous Reynolds stresses are replaced by their steady, time-mean values, providing a closed but nonlinear equation that "knows" about the underlying stationary state;

(ii) A purely linear response model that neglects all nonlinear and mean-flow interactions; and

(iii) A nonlinear model that evolves with self-advection but is completely ignorant of the stabilizing influence of the background eddy field.

The results demonstrate that, while the ensemble mean may conceptually represent the forced response of the system, one cannot simply obtain it by linear superposition of the forcing. The linear model reproduces the integrated energy variations but fails to capture the spatial evolution of the mean fields. The nonlinear response model, lacking any information about the stabilizing Reynolds-stress divergence, quickly develops its own chaotic dynamics—behaving more like an individual ensemble member than an ensemble mean. Only the frozen-turbulence model yields a bounded and physically realistic evolution: it remains stable for the amplitude of forcing perturbations studied here, performs reasonably well for the large-scale forcing of Case 1, but substantially overpredicts the ensemble-mean energy in the eddy-scale forcing of Case 2. The absence of feedback between the evolving mean and eddy statistics thus limits its validity to situations in which the energy exchange is slow and one-way.

These findings reinforce the view that parameterizations based solely on steady or time-mean statistics will be inadequate in systems where the eddy–mean exchange is intrinsically time dependent. In non-equilibrium regimes, the mean flow and fluctuations co-evolve, and their mutual adjustment must be represented explicitly if the correct amplitude and phasing of the ensemble mean are to be captured. From a practical standpoint, our experiments provide an *a posteriori* test of closure ideas: the steady-stress approximation works surprisingly well when the forcing acts at large scales but breaks down when the system is driven at the scales of its intrinsic variability. We argue that such *a posteriori* testings are crucial to avoid overfitting parameterizations to specific configurations (cf. Uchida et al., 2025a).

Looking more broadly, our results are consistent with the notion that the oceanic circulation resides in a regime between Case 1 and 2 where the forcing injects variability to the mean and eddy flow in dynamically active regions such as the separated western boundary currents and the Antarctic Circumpolar Current (Penduff et al., 2018; Uchida et al., 2022b; Hogg et al., 2022). The long-term goal of any parameterization scheme should therefore include representations of this intrinsic variability, not merely its mean imprint. Given that the ensemble mean structure is at least partially predictable, one may wonder whether it is possible to model the eddies that grow on top of such mean flow. Uchida et al. (2022a) and Deremble et al. (2023) are intriguing attempts at explicitly predicting the eddy flow in wind-driven gyres

$$\frac{\partial q^\dagger}{\partial t} + J(\psi^\dagger, q^\dagger) + \Big[J(\tilde{\psi}_{\mathrm{FT}} + \overline{\psi}, q^\dagger) + J(\psi^\dagger, \tilde{q}_{\mathrm{FT}} + \overline{q})\Big] = \mathscr{L}(q^\dagger) + \overline{J(\psi', q')}\,, \tag{14}$$

an approach which is sometimes referred to as superparameterizations where one explicitly models the sub-grid features (Khairoutdinov et al., 2005; Campin et al., 2011; Majda and Grooms, 2014)[1]. Interestingly, Eqs. (11) and (14) form a complete set to represent a single QG realization, $\boldsymbol{q}(\approx \overline{\boldsymbol{q}} + \widetilde{\boldsymbol{q}}_{\mathrm{FT}} + \boldsymbol{q}^\dagger)$, given the steady-state statistics, $\overline{(\cdot)}$. If we were to admit that the mean flow, $\widetilde{(\cdot)}$, evolves on a slower time scale than the eddy flow, $(\cdot)^\dagger$, we might be able to get away with coupling the two equations using separate time stepping between the two (somewhat analogous to the split in barotropic and baroclinic time stepping

[1] We have subtracted (4) and (11) from (1) to arrive at (14).

regularly adopted in GCMs; Marshall et al., 1997; Hallberg, 1997). We leave the examination on how this strategy fairs against an actual eddy-resolving simulation realized by solving for (1) for future work. There have been some promising efforts led by Mémin (2014); Li et al. (2023); Tissot et al. (2024) and Tucciarone et al. (2025) where they build upon such an idea of time-scale separation; the 'eddies' are modeled as random (in time, but spatially correlated) Brownian processes and use stochastic (Itô) calculus to account for their impact on the mean flow through spatial covariations.

We conclude on the remark that our ensemble experiments are highly idealized. Effects of bathymetry and vertical gradients of interior PV are not included in our flat-bottom two-layer configuration (Sterl et al., 2025; Lobo et al., 2025). Furthermore, the QG setting gives little to no consideration on the vertical velocity nor thermodynamics, which are key components in the ocean and climate system (Penduff et al., 2018; Griffies et al., 2015, 2024; Uchida et al., 2019, 2025a,b; Sun et al., 2025). Namely, the stratification does not drift in response to the forcing. All of such factors will modify the balance between forced and intrinsic variability in more realistic settings. Nevertheless, we expect that some of the fundamental features we find in QG settings to carry over to primitive-equation (PE) settings as QG dynamics comprise an important part of the full dynamics (Eady, 1949; Charney, 1971; Phillips, 1990; Vallis, 2006; Early et al., 2011; Kondrashov and Berloff, 2015; Uchida et al., 2023; Meunier et al., 2023; Deremble et al., 2023; Jamet et al., 2024). The basic lessons here appear robust: The evolution of the ensemble-mean depends not only on the external forcing but also on how energy is exchanged between the mean and fluctuating fields—a process that is fundamentally in non-equilibrium and central to the dynamics of the real ocean. It would be interesting to expand on our results by examining the ensemble-mean response to episodic forcing in stacked-shallow water and PE settings (Thiry et al., 2024; Zhang et al., 2025) but is beyond the scope of this study

## CONFLICT OF INTEREST STATEMENT

The authors declare no conflicts of interest.

## AUTHOR CONTRIBUTIONS

This study grew out from the many years of fruitful and exciting discussions with the late William Kurt Dewar. He is dearly missed but we hope he is enjoying many pints of IPA, bike tours, the Scottish snare and some ultimate Frisbee in the afterlife. Conceptualization of this study was done by W. Dewar (Dewar et al., 2024). Data curation was executed by A. Poje and B. Deremble. All authors contributed to the investigation and formal analyses were conducted by A. Poje. W. Dewar, A. Poje and T. Uchida wrote the original draft. All authors contributed to the editing of the final draft.

## FUNDING

W. Dewar was supported through National Science Foundation (NSF) grants OCE-1829856, OCE-1941963, OCE-2123632, and OCE-2023585, and the French 'Make Our Planet Great Again' (MOPGA) program managed by the Agence Nationale de la Recherche under the Programme d'Investissement d'Avenir, reference ANR-18-MPGA-0002. This MOPGA program, led by W. Dewar and T. Penduff between mid 2019 and late 2024, funded the postdoctoral activities by Q. Jamet, T. Uchida and L. Sun at l'Institut des Géosciences de l'Environnement (IGE) and several stays of W. Dewar at IGE over this period. T. Uchida also acknowledges support from the NSF grant OCE-2123632 and NASA award 80NSSC24K1649 during his time in the U.S. and the Moscow Institute of Physics and Technology Development Program (Priority-2030) upon moving to Russia. A. Poje acknowledges support from the NSF grant OCE-2123633. L. Sun is now supported from the NSF grant OCE-2123632. This research was also supported, in part, by a grant of computer time from the City University of New York High Performance Computing Center under NSF Grants CNS-0855217, CNS-0958379 and ACI-1126113.

## ACKNOWLEDGMENTS

Computational resources for producing the QG simulations and analyzing the outputs were provided by the CUNY High Performance Computing Center. We would like to thank Edward Peirce and Kelly Hirai for maintaining the FSU cluster on which some of the data were also analyzed.

## DATA AVAILABILITY STATEMENT

The QG model used in this study is available via Deremble et al. (2023, `https://github.com/bderembl/qgw`).

## APPENDIX A: SPECTRAL PROPER ORTHOGONAL DECOMPOSITION (SPOD) WITH QG ENERGY NORM

The analysis of the multi-layer quasi-geostrophic (QG) model's spatio-temporal dynamics was performed using a modified version of the Spectral Proper Orthogonal Decomposition (SPOD) procedure. This approach, while following the general framework of SPOD, was adapted to incorporate a physically relevant energy norm. This ensures that the resulting modes and their ranking are directly tied to the energetics of the system, providing a physically meaningful decomposition.

### General SPOD Procedure

The SPOD method, as formulated by Towne et al. (2018), provides a rigorous framework for identifying and ranking statistically stationary coherent structures by frequency. The procedure is based on the method of snapshots, but instead of analyzing instantaneous fields, it operates on the Fourier-transformed data. The core of the method is the computation and eigendecomposition of the **cross-spectral density (CSD)** matrix, which captures the average two-point correlations in the frequency domain.

Our implementation, adapted for the multi-layer quasi-geostrophic (QG) model, follows these steps:

1. **Data Segmentation**: A time series of $N$ snapshots, represented by the state vector $u(\mathbf{x}, t)$, is segmented into $N_b$ overlapping blocks. Each block, $u_k(\mathbf{x}, t)$, contains $N_t$ snapshots. This blocking allows for the use of a time-averaging ensemble, crucial for statistical convergence. In our two-layer model with $N_s = N_x \times N_y$ spatial points, the state vector at each time step, $u(t)$, is a column vector of $4N_s$ points, specifically containing the values of the potential vorticity $q_i$ and streamfunction $\psi_i$ for both layers:

$$u(t) = [q_1(t), \psi_1(t), q_2(t), \psi_2(t)]^T$$

   where the fields are stacked in column-vector form.
2. **Windowing**: A windowing function, such as a Hanning window, is applied to each block in time to minimize spectral leakage and improve the frequency resolution.

3. **Fourier Transform**: A discrete Fourier transform (DFT) is applied to each windowed block to transform the data into the frequency domain. This yields a set of Fourier-transformed snapshots, $\hat{u}_k(\mathbf{x}, \omega)$, for each block $k$ and frequency $\omega$.

### The Physically-Based Energy Norm and Weighting Matrix L

A critical deviation from the standard SPOD formulation is our use of a basin-averaged energy norm to define the inner product. This is essential for ensuring that the resulting modes are orthonormal with respect to the system's energy. In the context of our multi-layer QG model, the total energy of the system is the sum of the kinetic and potential energies, which can be expressed in terms of the streamfunction $\psi_i$ and potential vorticity $q_i$ for each layer $i$:

$$E = \sum_i \frac{1}{A} \iint_A - \{\psi_i q_i\} \, dA$$

To incorporate this energy norm into the discrete SPOD procedure, we define a weighting matrix, $\mathbf{L}$, such that the inner product between two state vectors, $\mathbf{u}$ and $\mathbf{v}$, is given by $\langle \mathbf{u}, \mathbf{v} \rangle = \mathbf{u}^* \mathbf{L} \mathbf{v}$. The matrix $\mathbf{L}$ is a block-diagonal matrix whose structure is determined by the energy equation. For our two-layer, uniform grid system, $\mathbf{L}$ is a $4N_s \times 4N_s$ matrix:

$$\mathbf{L} = \begin{bmatrix} \mathbf{0} & -\Delta A\mathbf{I} & \mathbf{0} & \mathbf{0} \\ -\Delta A\mathbf{I} & \mathbf{0} & \mathbf{0} & \mathbf{0} \\ \mathbf{0} & \mathbf{0} & \mathbf{0} & -\Delta A\mathbf{I} \\ \mathbf{0} & \mathbf{0} & -\Delta A\mathbf{I} & \mathbf{0} \end{bmatrix}$$

Here, $\Delta A$ is the constant area of a single grid cell and $\mathbf{I}$ is the $N_s \times N_s$ identity matrix. This matrix ensures that the SPOD analysis identifies and ranks modes based on their contribution to the total energy of the system, rather than on a generic mathematical norm.

### CSD Matrix and Eigenvalue Decomposition

4. **CSD Matrix Construction**: For each frequency $\omega$, the CSD matrix, $\mathbf{S}(\omega)$, is computed as an ensemble average of the outer product of the Fourier-transformed data from all blocks, **weighted by the matrix L**:

$$\mathbf{S}(\omega) = \frac{1}{N_b} \sum_{k=1}^{N_b} \hat{u}_k(\mathbf{x}, \omega) \mathbf{L} \hat{u}_k^*(\mathbf{x}, \omega)$$

   This explicit form of the CSD matrix calculation directly incorporates our energy norm.

5. **Eigenvalue Decomposition**: The CSD matrix is then decomposed into its eigenvalues and eigenvectors:

$$\mathbf{S}(\omega) \boldsymbol{\phi}_j(\mathbf{x}, \omega) = \lambda_j(\omega) \boldsymbol{\phi}_j(\mathbf{x}, \omega)$$

   The eigenvectors, $\boldsymbol{\phi}_j(\mathbf{x}, \omega)$, are the **SPOD modes**—spatially coherent structures that oscillate at frequency $\omega$. The corresponding eigenvalues, $\lambda_j(\omega)$, represent the energy of each mode at that frequency. By ranking the eigenvalues, we can identify the most energetic and dynamically significant structures in the system. The time-dependence of the modes is harmonic, given by $\Phi_j(\mathbf{x}, t) = \mathrm{Re}[\phi_j(\mathbf{x}, \omega)e^{i\omega t}]$.

## REFERENCES

Arbic, B., Muller, M., Richman, J., Shriver, J., Morten, A., Scott, R., et al. (2014). Geostrophic turbulence in the frequency-wavenumber domain: Eddy-driven low-frequency variability. *Journal of Physical Oceanography* 44, doi:10.1175/JPO–D–13–054.1

Berloff, P., Hogg, A. M. C., and Dewar, W. (2007). The turbulent oscillator: A mechanism of low-frequency variability of the wind-driven ocean gyres. *Journal of Physical Oceanography* 37, 2363 – 2386. doi:10.1175/JPO3118.1

Berloff, P. S. and McWilliams, J. C. (1999). Large-scale, low-frequency variability in wind-driven ocean gyres. *Journal of Physical Oceanography* 29, 1925–1949. doi:10.1175/1520-0485(1999)029<1925:LSLFVI>2.0.CO;2

Birkhoff, G. D. (1931). Proof of the ergodic theorem. *Proceedings of the National Academy of Sciences* 17, 656–660. doi:10.1073/pnas.17.12.656

Campin, J.-M., Hill, C., Jones, H., and Marshall, J. (2011). Super-parameterization in ocean modeling: Application to deep convection. *Ocean Modelling* 36, 90–101. doi:10.1016/j.ocemod.2010.10.003

Cessi, P. (2008). An energy-constrained parameterization of eddy buoyancy flux. *Journal of physical oceanography* 38, 1807–1819. doi:10.1175/2007JPO3812.1

Charney, J. G. (1971). Geostrophic turbulence. *Journal of the Atmospheric Sciences* 28, 1087–1095. doi:10.1175/1520-0469(1971)028<1087:GT>2.0.CO;2

Chen, R. and Flierl, G. R. (2015). The contribution of striations to the eddy energy budget and mixing: Diagnostic frameworks and results in a quasigeostrophic barotropic system with mean flow. *Journal of Physical Oceanography* 45, 2095–2113. doi:10.1175/JPO-D-14-0199.1

Deremble, B., Miller, L., and Albert, A. (2024). `qgw`*: Finite-differences QG model that relies on FFTW for the elliptic solver [Software]*

Deremble, B., Uchida, T., Dewar, W. K., and Samelson, R. M. (2023). Eddy-mean flow interaction with a Multiple-Scale Quasi Geostrophic model. *Journal of Advances in Modeling Earth Systems* doi:10.1029/2022MS003572

Dewar, W. K. (2003). Nonlinear midlatitude ocean adjustment. *Journal of physical oceanography* 33, 1057–1082. doi:10.1175/1520-0485(2003)033<1057:NMOA>2.0.CO;2

Dewar, W. K., Poje, A. C., Uchida, T., and Wienders, N. (2024). Characterizing ocean variability from months to years-mean vs eddies. In *American Geophysical Union, Ocean Sciences Meeting*. OP31H–04

Eady, E. T. (1949). Long waves and cyclone waves. *Tellus* 1, 33–52. doi:10.3402/tellusa.v1i3.8507

Early, J. J., Samelson, R., and Chelton, D. B. (2011). The evolution and propagation of quasigeostrophic ocean eddies. *Journal of Physical Oceanography* 41, 1535–1555. doi:10.1175/2011JPO4601.1

Eaves, R. E., Maddison, J. R., Marshall, D. P., and Waterman, S. (2025). An energy-and enstrophy-constrained parameterization of barotropic eddy potential vorticity fluxes. *Journal of Physical Oceanography* 55, 573–591. doi:10.1175/JPO-D-24-0027.1

Eden, C. and Greatbatch, R. J. (2008). Towards a mesoscale eddy closure. *Ocean Modelling* 20, 223–239. doi:10.1016/j.ocemod.2007.09.002

Farrell, B. F. and Ioannou, P. J. (2003). Structural stability of turbulent jets. *Journal of the Atmospheric Sciences* 60, 2101–2118. doi:10.1175/1520-0469(2003)060<2101:SSOTJ>2.0.CO;2

Fedele, G., Penduff, T., Pierini, S., Alvarez-Castro, M. C., Bellucci, A., and Masina, S. (2021). Interannual to decadal variability of the kuroshio extension: analyzing an ensemble of global hindcasts from a dynamical system viewpoint. *Climate Dynamics* 57, 975–992. doi:10.1007/s00382-021-05751-7

Ferrari, R., Griffies, S. M., Nurser, A. G., and Vallis, G. K. (2010). A boundary-value problem for the parameterized mesoscale eddy transport. *Ocean Modelling* 32, 143–156. doi:10.1016/j.ocemod.2010.01.004

Frisch, U. (1995). *Turbulence: The Legacy of A. N. Kolmogorov* (Cambridge: Cambridge University Press)

Gent, P. R. and McWilliams, J. C. (1990). Isopycnal mixing in ocean circulation models. *Journal of Physical Oceanography* 20, 150–155. doi:10.1175/1520-0485(1990)020<0150:IMIOCM>2.0.CO;2

Gent, P. R., Willebrand, J., McDougall, T. J., and McWilliams, J. C. (1995). Parameterizing eddy-induced tracer transports in ocean circulation models. *Journal of physical oceanography* 25, 463–474

Ghil, M., Allen, M. R., Dettinger, M. D., Ide, K., Kondrashov, D., Mann, M. E., et al. (2002). Advanced spectral methods for climatic time series. *Reviews of Geophysics* 40, 3–1–3–41. doi:10.1029/2000RG000092

Griffies, S. M., Adcroft, A., Beadling, R. L., Bushuk, M., Chang, C.-Y., Drake, H. F., et al. (2024). The GFDL-CM4X climate model hierarchy, Part I: model description and thermal properties. *Authorea Preprints* doi:10.22541/essoar.173282145.53065190/v1

Griffies, S. M., Winton, M., Anderson, W. G., Benson, R., Delworth, T. L., Dufour, C. O., et al. (2015). Impacts on ocean heat from transient mesoscale eddies in a hierarchy of climate models. *Journal of Climate* 28, 952–977. doi:10.1175/JCLI-D-14-00353.1

Grooms, I., Majda, A. J., and Smith, K. S. (2015). Stochastic superparameterization in a quasigeostrophic model of the Antarctic Circumpolar Currentz. *Ocean Modelling* 85, 1–15. doi:10.1016/j.ocemod.2014.10.001

Gu, Q., Gervais, M., Danabasoglu, G., Kim, W. M., Castruccio, F., Maroon, E., et al. (2024). Wide range of possible trajectories of North Atlantic climate in a warming world. *Nature communications* 15, 4221. doi:10.1038/s41467-024-48401-2

Haine, T. W., Griffies, S. M., Gebbie, G., and Jiang, W. (2025). A review of Green's function methods for tracer timescales and pathways in ocean models. *Journal of Advances in Modeling Earth Systems* 17, e2024MS004637. doi:10.1029/2024MS004637

Hallberg, R. (1997). Stable split time stepping schemes for large-scale ocean modeling. *Journal of Computational Physics* 135, 54–65. doi:10.1006/jcph.1997.5734

Hallberg, R. (2013). Using a resolution function to regulate parameterizations of oceanic mesoscale eddy effects. *Ocean Modelling* 72, 92–103. doi:10.1016/j.ocemod.2013.08.007

Hogg, A. M., Penduff, T., Close, S. E., Dewar, W. K., Constantinou, N. C., and Martínez-Moreno, J. (2022). Circumpolar variations in the chaotic nature of Southern Ocean eddy dynamics. *Journal of Geophysical Research: Oceans* 127, e2022JC018440. doi:10.1029/2022JC018440

Jamet, Q., Berger, A., Deremble, B., and Penduff, T. (2024). Thermodynamical Effects of Ocean Current Feedback in a Quasigeostrophic Coupled Model. *Journal of Physical Oceanography* 54, 1691–1704. doi:10.1175/JPO-D-23-0159.1

Jamet, Q., Leroux, S., Dewar, W. K., Penduff, T., Le Sommer, J., Molines, J.-M., et al. (2022). Non-local eddy-mean kinetic energy transfers in submesoscale-permitting ensemble simulations. *Journal of Advances in Modeling Earth Systems* doi:10.1029/2022MS003057

Khairoutdinov, M., Randall, D., and DeMott, C. (2005). Simulations of the atmospheric general circulation using a cloud-resolving model as a superparameterization of physical processes. *Journal of the Atmospheric Sciences* 62, 2136–2154. doi:10.1175/JAS3453.1

Kondrashov, D. and Berloff, P. S. (2015). Stochastic modeling of decadal variability in ocean gyres. *Geophysical Research Letters* 42, 1543–1553. doi:10.1002/2014GL062871

Kraichnan, R. H. (1976). Eddy viscosity in two and three dimensions. *Journal of Atmospheric Sciences* 33, 1521–1536. doi:10.1175/1520-0469(1976)033<1521:EVITAT>2.0.CO;2

Lembo, V., Lucarini, V., and Ragone, F. (2020). Beyond forcing scenarios: Predicting climate change through response operators in a coupled general circulation model. *Scientific Reports* 10, 8668. doi:10.1038/s41598-020-65297-2

Leroux, S., Penduff, T., Bessières, L., Molines, J.-M., Brankart, J.-M., Sérazin, G., et al. (2018). Intrinsic and atmospherically forced variability of the AMOC: Insights from a large-ensemble ocean hindcast. *Journal of Climate* 31, 1183–1203. doi:10.1175/JCLI-D-17-0168.1

Li, L., Deremble, B., Lahaye, N., and Mémin, E. (2023). Stochastic Data-Driven Parameterization of Unresolved Eddy Effects in a Baroclinic Quasi-Geostrophic Model. *Journal of Advances in Modeling Earth Systems* 15, e2022MS003297. doi:10.1029/2022MS003297

Lobo, M., Griffies, S. M., and Zhang, W. (2025). Vertical structure of baroclinic instability in a three-layer quasigeostrophic model over a sloping bottom. *Journal of Physical Oceanography* 55, 341–359. doi:10.1175/JPO-D-24-0130.1

Maddison, J. R. and Marshall, D. P. (2013). The Eliassen–Palm flux tensor. *Journal of Fluid Mechanics* 729, 69–102. doi:10.1017/jfm.2013.259

Majda, A. J. and Grooms, I. (2014). New perspectives on superparameterization for geophysical turbulence. *Journal of Computational Physics* 271, 60–77. doi:10.1016/j.jcp.2013.09.014

Mak, J., Maddison, J. R., Marshall, D. P., Ruan, X., Wang, Y., and Yeow, L. (2023). Scale-awareness in an eddy energy constrained mesoscale eddy parameterization. *Journal of Advances in Modeling Earth Systems* 15, e2023MS003886. doi:10.1029/2023MS003886

Mak, J., Marshall, D. P., Maddison, J. R., and Bachman, S. D. (2017). Emergent eddy saturation from an energy constrained eddy parameterisation. *Ocean Modelling* 112, 125–138. doi:10.1016/j.ocemod.2017.02.007

Marshall, D. P., Maddison, J. R., and Berloff, P. S. (2012). A framework for parameterizing eddy potential vorticity fluxes. *Journal of Physical Oceanography* 42, 539–557. doi:10.1175/JPO-D-11-048.1

Marshall, J., Hill, C., Perelman, L., and Adcroft, A. (1997). Hydrostatic, quasi-hydrostatic and non-hydrostatic ocean modelling. *Journal of Geophysical Research* 102, 5733–5753. doi:10.1029/96JC02776

Marston, J. B., Chini, G. P., and Tobias, S. M. (2016). Generalized quasilinear approximation: Application to zonal jets. *Physical Review Letters* 116, 214501. doi:10.1103/PhysRevLett.116.214501

McWilliams, J. C. (2006). *Fundamentals of Geophysical Fluid Dynamics* (Cambridge: Cambridge University Press)

Mémin, E. (2014). Fluid flow dynamics under location uncertainty. *Geophysical & Astrophysical Fluid Dynamics* 108, 119–146. doi:10.1080/03091929.2013.836190

Meunier, J., Miquel, B., and Gallet, B. (2023). A direct derivation of the Gent–McWilliams/Redi diffusion tensor from quasi-geostrophic dynamics. *Journal of Fluid Mechanics* 963, A22. doi:10.1017/jfm.2023.347

Narinc, O., Penduff, T., Maze, G., Leroux, S., and Molines, J.-M. (2024). North Atlantic Subtropical Mode Water properties: intrinsic and atmospherically forced interannual variability. *Ocean Science* 20, 1351–1365. doi:10.5194/os-20-1351-2024

Penduff, T., Sérazin, G., Leroux, S., Close, S., Molines, J.-M., Barnier, B., et al. (2018). Chaotic variability of ocean heat content: Climate-relevant features and observational implications. *Oceanography* 31, 63–71. doi:10.5670/oceanog.2018.210

Phillips, N. A. (1990). The emergence of quasi-geostrophic theory. In *The Atmosphere—A Challenge: The Science of Jule Gregory Charney* (Springer). 177–206. doi:10.1007/978-1-944970-35-2_11

Pierini, S. (2020). Statistical significance of small ensembles of simulations and detection of the internal climate variability: An excitable ocean system case study. *Journal of Statistical Physics* 179, 1475–1495. doi:10.1007/s10955-019-02409-x

Romanou, A., Rind, D., Jonas, J., Miller, R., Kelley, M., Russell, G., et al. (2023). Stochastic bifurcation of the North Atlantic Circulation under a mid-range future climate scenario with the NASA-GISS modelE. *Journal of Climate* , 1–49doi:10.1175/JCLI-D-22-0536.1

Sérazin, G., Jaymond, A., Leroux, S., Penduff, T., Bessières, L., Llovel, W., et al. (2017). A global probabilistic study of the ocean heat content low-frequency variability: Atmospheric forcing versus oceanic chaos. *Geophysical Research Letters* 44, 5580–5589. doi:10.1002/2017GL073026

Serazin, G., Penduff, T., Gregorio, S., Barnier, B., Molines, J., and Terray, L. (2015). Intrinsic variability of sea level from global ocean simulations: Spatiotemporal scales. *Journal of Climate* 10, 4279–4292

Simonnet, E. (2005). Quantization of the low-frequency variability of the double-gyre circulation. *Journal of Physical Oceanography* 35, 2268 – 2290. doi:10.1175/JPO2806.1

Simonnet, E., Ghil, M., Ide, K., Temam, R., and Wang, S. (2003). Low-frequency variability in shallow-water models of the wind-driven ocean circulation. Part II: Time-dependent solutions. *Journal of physical oceanography* 33, 729–752. doi:10.1175/1520-0485(2003)33<729:LVISMO>2.0.CO;2

Smagorinsky, J. (1963). General circulation experiments with the primitive equations: I. the basic experiment. *Monthly weather review* 91, 99–164. doi:10.1175/1520-0493(1963)091<0099:GCEWTP>2.3.CO;2

Sterl, M. F., Palóczy, A., Groeskamp, S., Baatsen, M. L., LaCasce, J. H., and Isachsen, P. E. (2025). The joint effects of planetary, topography and friction on baroclinic instability in a two-layer quasi-geostrophic model. *Journal of Fluid Mechanics* 1012, A1. doi:10.1017/jfm.2025.10172

Sun, L., Uchida, T., Penduff, T., Dewar, W. K., Deremble, B., Poje, A. C., et al. (2025). On the dynamics of the subtropical mode water from an ensemble view. *Authorea Preprints* doi:10.22541/essoar.174802928.80389595/v1

Takasuka, D., Suematsu, T., Miura, H., and Nakano, M. (2025). Propagation of the Madden-Julian oscillation as a deterministic chaotic phenomenon. *ArXiv* doi:10.48550/arXiv.2506.23195

Taylor, G. I. (1938). The spectrum of turbulence. *Proceedings of the Royal Society of London. Series A-Mathematical and Physical Sciences* 164, 476–490. doi:10.1098/rspa.1938.0032

Thiry, L., Li, L., Mémin, E., and Roullet, G. (2024). A unified formulation of quasi-geostrophic and shallow water equations via projection. *Journal of Advances in Modeling Earth Systems* 16, e2024MS004510. doi:10.1029/2024MS004510

Tissot, G., Mémin, É., and Jamet, Q. (2024). Stochastic compressible Navier–Stokes equations under location uncertainty. In *Stochastic Transport in Upper Ocean Dynamics II* (Springer Nature Switzerland), vol. 11. 293–319

Towne, A., Meidner, M., and Schmid, P. J. (2018). Spectral proper orthogonal decomposition of turbulent flows. *Journal of Fluid Mechanics* 847, 821–857. doi:10.1017/jfm.2018.328

Tucciarone, F. L., Li, L., Mémin, E., and Chandramouli, P. (2025). Derivation and numerical assessment of a stochastic large-scale hydrostatic primitive equations model. *Journal of Advances in Modeling Earth Systems* doi:10.1029/2024MS004783

Uchida, T., Balwada, D., Abernathey, R. P., McKinley, G. A., Smith, K. S., and Lévy, M. (2019). The contribution of submesoscale over mesoscale eddy iron transport in the open Southern Ocean. *Journal of Advances in Modeling Earth Systems* 11, 3934–3958. doi:10.1029/2019MS001805

Uchida, T., Balwada, D., Jamet, Q., Dewar, W. K., Deremble, B., Penduff, T., et al. (2023). Cautionary tales from the mesoscale eddy transport tensor. *Ocean Modelling* 182, 102172. doi:10.1016/j.ocemod.2023.102172

Uchida, T., Bodner, A. S., Reichl, B. G., Adcroft, A., Fox-Kemper, B., Ilicak, M., et al. (2025a). Representation of surface mixed-layer eddies affects the large-scale ventilation of the global ocean. *Authorea Preprints* doi:10.22541/essoar.174802994.41704767/v1

Uchida, T., Deremble, B., Dewar, W. K., and Penduff, T. (2021a). Diagnosing the Eliassen-Palm flux from a quasi-geostrophic double gyre ensemble. In *EarthCube Annual Meeting* (NSF). doi:10.5281/zenodo.5496375

Uchida, T., Deremble, B., and Penduff, T. (2021b). The seasonal variability of the ocean energy cycle from a quasi-geostrophic double gyre ensemble. *Fluids* 6, 206. doi:10.3390/fluids6060206

Uchida, T., Deremble, B., and Popinet, S. (2022a). Deterministic model of the eddy dynamics for a midlatitude ocean model. *Journal of Physical Oceanography* 52, 1133–1154. doi:10.1175/JPO-D-21-0217.1

Uchida, T., Jamet, Q., Dewar, W. K., Balwada, D., Le Sommer, J., and Penduff, T. (2022b). Diagnosing the thickness-weighted averaged eddy-mean flow interaction in an eddying North Atlantic ensemble: The Eliassen–Palm flux. *Journal of Advances in Modeling Earth Systems* 14, e2021MS002866. doi:10.1029/2021MS002866

Uchida, T., Jamet, Q., Dewar, W. K., Deremble, B., Poje, A. C., and Sun, L. (2024a). Imprint of chaos on the ocean energy cycle from an eddying North Atlantic ensemble. *Journal of Physical Oceanography* 54, 679–696. doi:10.1175/JPO-D-23-0176.1

Uchida, T., Jamet, Q., Poje, A. C., Wienders, N., and Dewar, W. K. (2024b). Wavelet-based wavenumber spectral estimate of eddy kinetic energy: Application to the North Atlantic. *Ocean Modelling* 190, 102392. doi:10.1016/j.ocemod.2024.102392

Uchida, T., Jamet, Q., Poje, A. C., Wienders, N., Sun, L., and Dewar, W. K. (2025b). Dynamics and thermodynamics of the Boussinesq North Atlantic eddy kinetic energy spectral budget. *Journal of Advances in Modeling Earth Systems* 17, e2024MS004781. doi:10.1029/2024MS004781

Vallis, G. (2006). *Atmospheric and Oceanic Fluid Dynamics* (Cambridge)

Veronis, G. (1963). An analysis of wind-driven ocean circulation with a limited number of Fourier components. *Journal of Atmospheric Sciences* 20, 577–593

Wei, H., Wang, Y., and Mak, J. (2024). Parameterizing eddy buoyancy fluxes across prograde shelf/slope fronts using a slope-aware Geometric closure. *Journal of Physical Oceanography* 54, 359–377. doi:10.1175/JPO-D-23-0152.1

Young, W. (2012). An exact thickness-weighted average formulation of the Boussinesq equations. *Journal of Physical Oceanography* 42, 692–707. doi:10.1175/JPO-D-11-0102.1

Zhang, W., Kuo, Y.-H., Silvestri, S., Adcroft, A., Hallberg, R. W., and Griffies, S. M. (2025). A WENO finite-volume scheme for the evolution of potential vorticity in isopycnal ocean models. *Authorea Preprints* doi:10.22541/essoar.175380391.18723979/v1

Zhao, M., Ponte, R. M., Penduff, T., Close, S., Llovel, W., and Molines, J.-M. (2021). Imprints of ocean chaotic intrinsic variability on bottom pressure and implications for data and model analyses. *Geophysical Research Letters* 48, e2021GL096341. doi:10.1029/2021GL096341